

Chapter 14

2.8 GA BONINITE-HOSTING PARTIAL SUPRASUBDUCTION ZONE OPHIOLITE SEQUENCES FROM THE NORTH KARELIAN GREENSTONE BELT, NE BALTIC SHIELD, RUSSIA

A.A. SHCHIPANSKY^a, A.V. SAMSONOV^b, E.V. BIBIKOVA^c,
LI. BABARINA^a, A.N. KONILOV^a, K.A. KRYLOV^{a,1},
A.I. SLABUNOV^d AND M.M. BOGINA^b

^a*Geological Institute of RAS, Pyzhevsky per., 7, Moscow, 109017, Russia*

^b*Institute of Ore Deposits, Petrography, Geochemistry and Mineralogy of RAS, Staromonetny per., 35, Moscow, 109017, Russia*

^c*Vernadsky Institute of Geochemistry and Analytical Chemistry of RAS, Kosygin St., 19, Moscow, 17975, Russia*

^d*Karelian Research Center of RAS, Institute of Geology, Pushkinskaya St., 11, Petrozavodsk, 185610, Karelia, Russia*

Neoproterozoic subduction-related assemblages of the North Karelian greenstone belt, in the NE part of the Baltic Shield, Russia, contain the world's oldest known boninite series, occurring in at least in two areas of the belt. The first area, referred to here as the Khizovaara structure, shows evidence of a late Archean ocean-island volcanic arc collage formed during two tectonic episodes nearly 2.8 Ga ago. The second area, named the Iringora structure, preserves distinctive features of an ophiolite pseudostratigraphy, including not only gabbro and lava units, but also remnants of a sheeted dike complex. The major and trace element chemistry of the Iringora ophiolitic gabbro, dike and lava units suggests a comagmatic series with a continuous compositional variation from more primitive mafic to strictly boninitic melts. In terms of major- and trace element abundance, the boninite series of the North Karelian greenstone belt is practically indistinguishable from the Group I and II of the Troodos upper pillow lavas. These occurrences strongly suggest that Neoproterozoic subduction-related processes including boninite-hosting supra-subduction zone ophiolites have not changed substantially over the past 2.8 Ga.

¹Present address: Department of Geological and Environment Sciences, Stanford University, CA 94305-2115, USA.

1. INTRODUCTION

Many ophiolites with arc geochemical signatures are thought to have formed as oceanic type crust above subduction zones. These have been termed suprasubduction zone (SSZ) ophiolites (Pearce et al., 1984). The latter are recognized frequently in Phanerozoic orogenic belts, but seldom if ever in the early Precambrian. Until recently (Kusky et al., 2000) there were no examples of Archean mafic-ultramafic sequences for which one could consider the most likely origin to be oceanic (Bickle et al., 1994). In addition to that, boninite rocks have also not been reported for the Archean (e.g., Sylvester et al., 1997; see also Polat and Kerrich, 2004). Amongst all rock types, boninites, perhaps, are the only rocks which are almost exclusively associated with ophiolites, but not necessarily vice versa (Cameron et al., 1979).

Boninitic rocks, or boninite series (Meijer, 1980) volcanic suites *sensu lato*, are commonly believed to be unusually sensitive indicators of supra-subduction zone mantle wedge processes (Crawford et al., 1989). They are unique because they have appropriate major element chemical compositions thought to be primary magmas from partial melting of the peridotite mantle wedge above the downgoing lithospheric slab (Fallon and Crawford, 1991). Thus the occurrence of boninite lavas in ancient arc-related assemblages has important tectonic implications.

One possible explanation for lack of Archean boninitic volcanism is that higher heat flow in the Archean may have caused subducted oceanic crust to have partially melted rather than forming dehydrating reactions characteristic of modern subduction zones (e.g., McCulloch, 1993). If so, Archean subduction zones could have been flat and slabs been largely disaggregated in the upper mantle at depths less than 200 km (Martin, 1986; Abbott et al., 1994). Recently, the few occurrences of boninites have been described from the Paleoproterozoic (Poidevin, 1994; Wyman, 1999). Fan and Kerrich (1997) and Kerrich et al. (1998) have reported a 2.7 Ga low-Ti tholeiite association of boninite series akin to ophiolitic basalts of Sun and Nesbitt (1978). Among these examples only the 1.9 Ga Amisk boninite series of the Trans-Hudson Orogen in Canada occurs in an ophiolite-like setting (Wyman, 1999). The older boninite series of the Bogoin belt (2.3 Ga) and of the Abitibi belt (2.7 Ga) are associated with komatiites which are absent from Phanerozoic SSZ ophiolites. This, in turn, suggests a possible mantle plume input in the origin of those occurrences (Poidevin, 1994; Kerrich et al., 1998).

This paper reports detailed data for 2.8 Ga boninitic occurrences from the North Karelian greenstone belt (Russia) including the Khizovaara and Iringora Structures (Shchipan-sky, 1999, 2001). These display geological and geochemical traits similar with some well-known Phanerozoic SSZ ophiolites providing unique insight for understanding crust-forming processes from early Earth.

2. GEOLOGY

The Archean domain of the Baltic (Fennoscandian) shield traditionally is divided into three distinct parts (Fig. 1). The northern, Lapland-Kola province mainly consists

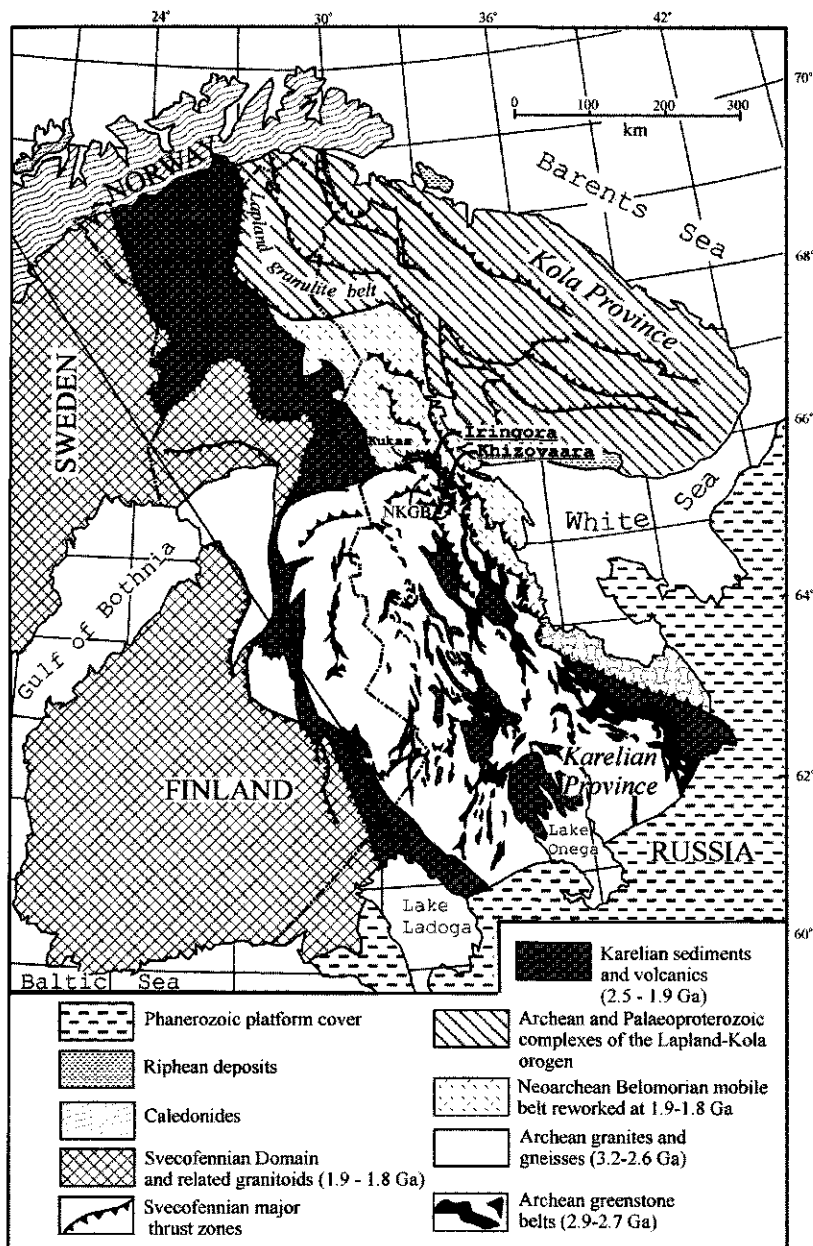


Fig. 1. Main tectonic units in the eastern part of the Baltic shield showing the location of the Khizovaara and Iringora Structures. Abbreviation: NKGB = North Karelian greenstone belts.

of several previously dispersed Archean crustal terranes that together with the different Paleoproterozoic belts have been involved in a collisional-type orogeny at 2.0 to 1.9 Ga (Bridgwater et al., 2001). A central, NW-trending segment known as the Belomorian mobile belt is occupied by assemblages of gneisses and amphibolites. This part of the Baltic Shield has experienced two major orogenic periods, in the Neoproterozoic and Paleoproterozoic. The Neoproterozoic period included several crust-forming events between c. 2.9 and 2.7 Ga which can be interpreted in terms of first subduction-related and later collisional orogeny (e.g., Gaál and Gorbatshev, 1987; Bibikova et al., 1996). In the end of the Paleoproterozoic (c. 1.9–1.8 Ga ago) strong tectonothermal reworking occurred during an event of crustal stacking and thrusting referred to as the Svecofennian orogeny which was caused by other thrusting of Lapland granulite belt onto the Belomorian belt (e.g., Bibikova et al., 1996, 2001; Bogdanova, 1996). Although the Svecofennian high-grade metamorphism and folding affected all of the belt, its major Neoproterozoic crustal structure reveals that early thrust and fold nappes developed c. 2.74–2.70 Ga (Miller and Mil'kevich, 1995). In contrast, the Karelian province displays no isotopic evidence for strong Paleoproterozoic reworking (Bibikova et al., 2001). The Karelian craton forms the core of the shield and largely consists of volcanic and sedimentary rocks (greenstones) and granites/gneisses that formed between 3200 and 2600 Ma and were dominantly metamorphosed at low-grade (Lobach-Zhuchenko et al., 1993; Sorjonen-Ward et al., 1997). Local synformal patches of Paleoproterozoic (2.45 to 1.9 Ga) volcano-sedimentary rocks unconformably overlie the Karelian basement. To the southwest of the Archean Karelian craton, the Svecofennian domain represents a large portion of Paleoproterozoic crust developed between 2.0 and 1.75 Ga (Gaál and Gorbatshev, 1987).

Although tectonic settings of the Karelian Archean greenstone belts are still a matter of debate, there are some indications for subduction-accretion processes that had operated, at least, since c. 2.9 Ga (e.g., Puchtel et al., 1998, 1999). However, a large involvement of deep mantle-plume derived oceanic plateaus into Archean crustal growth processes remains questionable in a respect of subduction style. New lines of evidence on Archean subduction-related environments come from the North Karelian greenstone belt.

2.1. North Karelian Greenstone Belt

The North Karelian greenstone belt (= NKGB for brevity) extends for 300 km along the boundary between the Karelian granite-greenstone terrain and the Belomorian mobile belt (Fig. 1). It is comprised of several greenstone belts isolated each from other by granitoids or unexposed areas. All belts preserve similar lithologies and structural styles. Thus they represent the fragments of a single Neoproterozoic unimodal greenstone belt (Kozhevnikov, 1992, 2000). U-Pb dating of titanites and rutiles shows that the NKGB is located near the inside boundary of the Svecofennian frontal thrusting directed toward the Karelian craton (Bibikova et al., 2001). Superimposed events include medium- to high-grade metamorphism of the moderate- to high-pressure facies series. However, only minor crustal additions accompanied Paleoproterozoic tectonism within the Karelian-Belomorian border zone. In contrast to the Belomorian mobile belt, here there is no evidence for em-

placement of Paleoproterozoic granites or magmatites. Post-Archean igneous activity is restricted to scarce swarms of gabbro-dioritic dikes and slightly dismembered gabbro-noritic sills. These are age equivalent to c. 2.45–2.40 Ga mafic intrusions widely distributed throughout both the Belomorian and Karelian parts of the Baltic Shield (Amelin et al., 1995). The entire Belomorian belt strikingly lacks the extensive Paleoproterozoic volcano-sedimentary cover that characterizes substantial parts of the Karelian craton. This cover could be wholly eroded from the Svecofennian mountain belt thus exposing a deeper crustal level than its Karelian neighbour (Bogdanova, 1996). The only remnant of the Paleoproterozoic supracrustal sequence is preserved within the Kukasozero belt that extends along the Karelian-Belomorian border zone. The belt provides important information on the Paleoproterozoic structural development (Babarina, 1998) that has been largely used in this study to assess its overprinting effect onto Neoproterozoic structural patterns of the NKGB.

The NKGB has been the subject of comprehensive field studies that define the basic geological and geochemical characteristics of the belt, interpreted to be a Neoproterozoic accretionary orogen (Kozhevnikov, 1992, 2000). All unit terms used in this study are modified from Kozhevnikov (2000).

2.2. *Khizovaara Structure*

The Khizovaara greenstone structure is a small but well exposed part of the NKGB. It is made up dominantly of a variety of volcanic rocks bordered on both sides by tonalitic intrusions. All of the Khizovaara rocks have experienced polyphase deformation and low-amphibolite facies metamorphism, but the deformation is heterogeneous and volcanic textures are occasionally preserved, so igneous nomenclature is used. The prefix meta is implicit below. Its structural pattern appears to be an imbricate south-dipping homocline clearly displaying the contrasting lithologic assemblages (Fig. 2). The northern flank essentially consists of a sediment-free mafic volcanic sequence referred to as the Northern assemblage, whereas the southern flank largely displays acid-felsic volcanic and volcanoclastic rocks combined into the Southern assemblage. In addition, local piles of the so-called, upper pillowed tholeiitic basalts overlie unconformably (Thurston and Kozhevnikov, 2000) or are thrust imbricated on top of the acid-felsic volcanogenic assemblage. The tectonostratigraphy of the entire Khizovaara sequence is summarized in Fig. 3.

Northern lithotectonic assemblage. This can be subdivided into four volcanogenic units based on differences in outcrop appearance, petrography and geochemistry. The northernmost and likely oldest volcanic unit in the Khizovaara Structure outcrops as a sequence of volcanics and gabbro sills of IAT-like affinity. Rarely preserved pillow textures and the absence of interflow sediments suggest their submarine and probable deep-water origin. Two separate small bodies of highly deformed peridotites are located at the base of the unit (Kozhevnikov, 1992) but their relationships with the lower tholeiites are unknown. Boninite series volcanics structurally and stratigraphically (?) overlie the lower tholeiites. The boundary between the two units is abrupt and is marked by a sudden appearance of primitive low-Ti high-Mg tholeiites. These rocks are described in detail below, because of

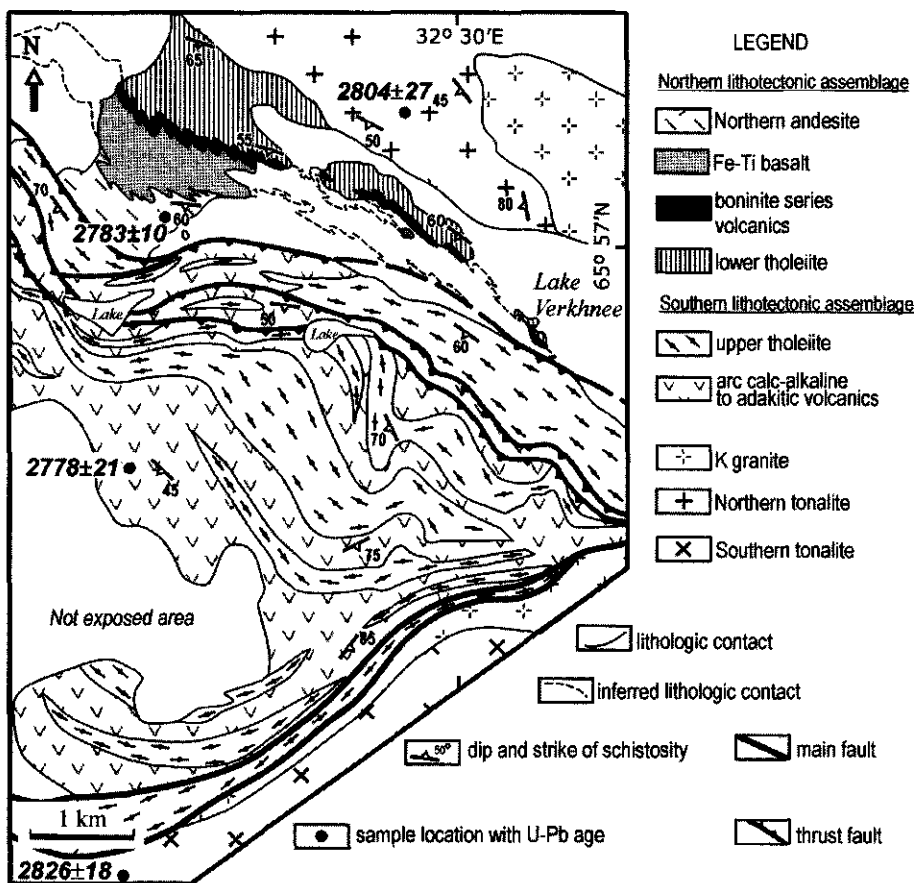
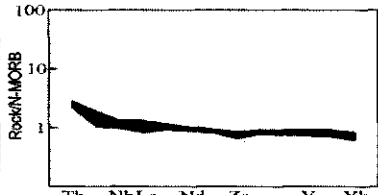
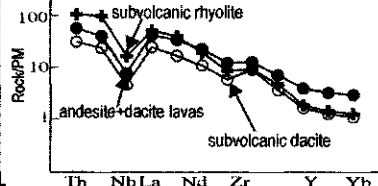
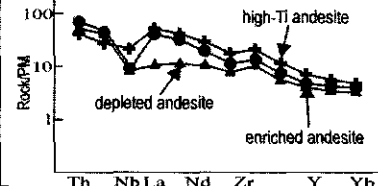
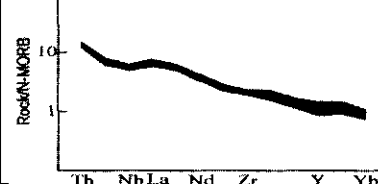
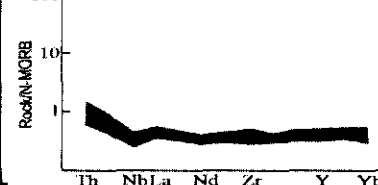
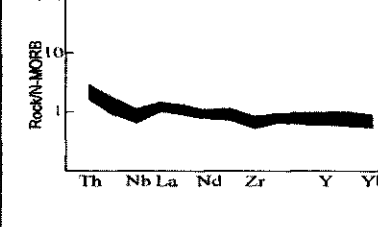


Fig. 2. Geological map of the Khizovaara Structure (compiled by authors using data of Kozhevnikov, 1992, 2000, and Thurston and Kozhevnikov, 2000).

their paucity in the Archean terrains. Farther south and structurally higher still, yet another mafic volcanic unit consists of ferro-tholeiitic basalts strongly enriched in incompatible trace element abundances compared to the lower volcanic units. Its contacts with both the underlying and overlying units are tectonic and marked by occurrence of the relatively wide (up to 20–30 m) zones of highly deformed rocks unusually rich in garnet. Furthermore, there is no evidence that the intrusive rocks related to the ferro-tholeiitic basalts,

Fig. 3. Tectonostratigraphy, U-Pb zircon ages and main geochemical characteristics of the Khizovaara sequence. Arrows indicate the thrust boundaries. Abbreviations: PM, primitive mantle abundance; N-MORB, normal mid-ocean ridge basalt abundance after Hofmann (1988).

AGE (Ma)		Lithologies	Main trace-element characteristics
<p>2778 ± 21</p>	<p>Southern (upper) lithotectonic assemblage</p>	<p><u>Upper metatholeiites</u> of MORB-like affinity. Pillowed and massive basalt and andesite-basalt flow. Co-magmatic shallow-level gabbro sills. Rare thin bodies of metapicrites of unclear affinity. Thickness up to 500-600 m.</p>	
		<p><u>Southern metaandesite-dacite-rhyolite unit.</u> Lava flows, pyroclastic horizons, rudaceous felsic volcanoclastics. Siliciclastic turbidites, thin lense of carbonaceous schists and quartz arenites. Thickness up to 1000 m.</p>	
<p>2783 ± 10</p>	<p>Northern lithotectonic assemblage</p>	<p><u>Northern metaandesites.</u> Amygdaloidal and massif lavas, coarse pyroclastic horizons. Geochemically they are high-Mg and both depleted and enriched in trace element abundance. Thickness up to 300-400 m.</p>	
		<p><u>Fe-Ti metabasalts</u> of OIB-like affinity. Massive flows and co-magmatic shallow-level gabbro sills. Thickness up to 400-500 m.</p>	
<p>> 2804 ± 27</p>	<p>Northern (lower) lithotectonic assemblage</p>	<p><u>Boninite series</u> metavolcanics. Thickness up to 50 m. Dominantly lavas facies including both the low-Ti high-Mg primitive basalts and high-Ca boninites. Rare felsic dikes of boninitic affinity.</p>	
		<p><u>Lower metatholeiites</u> of island arc affinity. Up to 400 m thickness sediment-free sequence of lavas and subordinate shallow-level gabbro sills. Small bodies of metaperidotites at the base of unit.</p>	

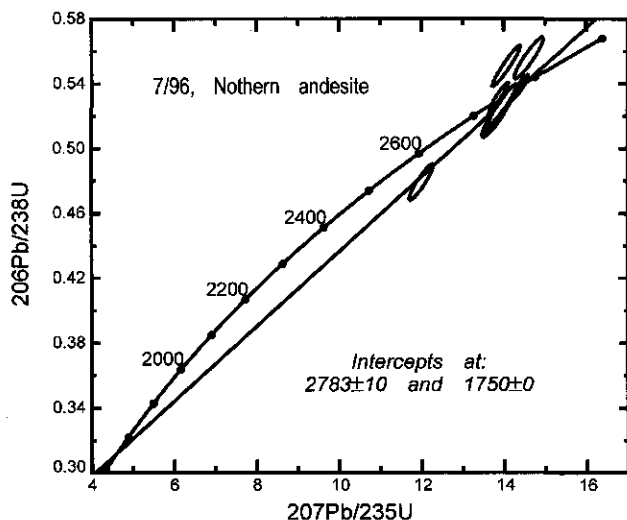


Fig. 4. NORDSIM ionprobe result for the northern andesite (sample 7/96) from the Khizovaara structure.

i.e., sills or dikes, take place within other volcanic units. It may indicate that originally they formed a separate volcanic pile which was consequently incorporated into a single imbricate stack during later accretionary events. Numerous tonalitic dikes cutting all units of the lower mafic assemblage have yielded an U-Pb discordant age of 2803 ± 35 Ma (Kozhevnikov, 1992). These dikes obviously derive from the northern tonalitic intrusion which shows a similar U-Pb age of 2804 ± 27 Ma.

Yet another group of volcanic rocks called the Northern andesites completes the lower lithotectonic assemblage. This includes mostly high-Mg andesite and subordinate andesite-dacite metavolcanics clearly distinguished from the Southern counterparts both by their field occurrence and unusual geochemical characteristics. Macroscopically they are amygdaloidal, massive and partly coarse, fragmental acid metavolcanic rocks developed in a subaerial-subaqueous environment (Thurston and Kozhevnikov, 2000). Ionprobe U-Pb dating of a homogeneous magmatic zircon from the Northern andesite yields a concordant age of 2783 ± 10 Ma (Fig. 4).

It is interesting that due to deformational and metamorphic transformations the quartz and quartz-plagioclase amygdales broke into roughly cylindrical, pencil-like crystal aggregates thus providing good strain markers. Based on a wide range of strain determination made on the amygdaloidal andesites, Kozhevnikov (2000) has assessed that constrictional strains range between 300% and 680%.

Southern lithotectonic assemblage. The contact of the Southern lithotectonic assemblage with the underlying Northern assemblage is largely obscured by subsequent Svecofennian overthrusting events. This assemblage largely consists of both wedge- and slab-derived volcanogenic rocks developed in a mature island arc setting. These comprise

a variety of andesite-dacite-rhyolite lava flows accompanied by fine- to coarse-grained volcano-sedimentary rocks. A number of semi-simultaneous dacitic and rhyolitic dykes and sills are scattered throughout the effusive facies volcanics. The concordant U-Pb age of 2778 ± 21 Ma for zircons from the Southern felsic lavas defines the time of their emplacement. Volcano-sedimentary rocks dominantly consist of interbedded siliciclastic rocks displaying in some places moderate sorting and graded bedding with alumina-enriched upper parts, all indicative for sediments deposited by turbidity currents (Thurston and Kozhevnikov, 2000). Minor but prominent components of the volcano-sedimentary sequence include several thin horizons of carbonaceous schists and quartz arenites. The latter have recently been studied in detail by Thurston and Kozhevnikov (2000) and interpreted to have formed in a shallow water environment during the late stage of arc volcanism.

The upper tholeiite unit is included in the Southern lithotectonic assemblage based only in its positions in the thrust stack. It is composed of pillowed and massive lava flows of tholeiitic basalt and andesite-basalt compositions accompanied by co-magmatic gabbro sills. As opposed to the lower tholeiites, they display flat trace element patterns without negative Nb anomalies and tend to be geochemically similar to N-MORB basalts. Amongst the basalts there are also rare thin bodies of picritic rocks of unclear affinity.

The Southern lithotectonic assemblage is flanked to the south by a wide shear zone along the diorite-granodiorite pluton contact. In contrast to the age determination on the felsic volcanics, it displays a somewhat older U-Pb upper-intercept zircon age of 2826 ± 18 Ma indicating a possible contribution of an older crustal component. A few intrusions of coarse-grained gneissose feldspar granites post-date all the above Khizovaara volcanic and igneous suites.

Structural development. As shown in Fig. 2, the Khizovaara greenstone sequence comprises steeply dipping and thin-skinned shortened volcanogenic assemblages displaying structural patterns typical of an imbricate fold-thrust wedge (e.g., Kusky and Vearncombe, 1997). Moreover the Southern lithotectonic assemblage was subjected to south-directed overthrusting onto the Northern assemblage. The latter event and subsequent intense shearing along the greenstone margins was obviously due to the Svecofennian stacking indicated by the Khizovaara titanite and rutile U-Pb ages of 1750 Ma (Bibikova et al., 2001). Because of the complex and superimposed Svecofennian deformations accompanied by the relatively high temperature metamorphism, recognition of earlier structural development is problematical. Nevertheless Kozhevnikov (1992) has found some indications of earlier tectonic fabrics and identified three deformation stages for the Archean structural development of the Khizovaara sequence. The earliest D_1 stage is found in the Northern lithotectonic assemblage and includes the earliest thrust faulting predating the emplacement of the tonalitic dikes. Second-generation or D_2 structures are well exposed in the Southern acid-felsic volcanogenic assemblage. They are dominated by coeval mesoscopic- to the map-scale EW and NE-trending closed folds possibly associated with thrust faults. The D_3 stage includes at least four folding events collectively characterized by development of NE to NW-trending upright folds.

2.3. Boninite Series: Field Occurrence, Petrography and Mineral Chemistry

To the author's knowledge, medium- to high-grade metamorphosed boninites have not formerly been petrologically described in Archean domains, or in younger regions in general. Thus it is of particular interest to describe the unique Khizovaara metaboninitic rocks in detail.

The Khizovaara boninite series rocks are exposed as a sequence up to 50 m thick (Fig. 2). Its present thickness obviously is not primary because it is strongly stretched parallel to layering and flattened perpendicular to layering. Kozhevnikov (1992, 2000) estimates that the original thickness of this unit could be at least 4–5 times thicker than the present thickness.

The boninite series metavolcanics appear as distinct pistachio-green amphibolite in the field. They include the more abundant low-Ti ($\text{TiO}_2 < 0.5\%$) high-Mg metatholeiites and the more evolved, strictly metaboninitic rocks, collectively forming a coherent low-Ti volcanic series akin to the high-Ca boninite series of some well-known Phanerozoic counterparts (e.g., Cameron, 1985; Smellie et al., 1995). Notice that it is impossible to distinguish between low-Ti tholeiitic and boninitic amphibolites based on macroscopic field appearance alone. Yet the most evolved members of the boninite series containing up to 60 wt% SiO_2 show no clear visual differences with the low-Ti high-Mg amphibolites. Thus, based on limited sampling, these amphibolites were previously described as komatiitic and komatiitic basalt lavas interpreted to have formed in a mafic plateau volcanic setting (Thurston and Kozhevnikov, 2000). However they do not display indications for the presence of amphibole or olivine spinifex textures, typical of volcanic rocks of komatiitic affinity. Only scarce signs of primary volcanic textures exist, including remnants of small pillows and thin-bedded interflow (?) horizons of the same composition, perhaps representing a highly stretched hyaloclastitic material. In addition, there are only a few of stretched-out sheet-like bodies that are distinctly different from other units by their light-grey color discordant in relationships with the metalavas. They are interpreted, on both the field and geochemical grounds, as remnants of late felsic dikes of boninitic affinity. Thus we emphasize that metaboninitic rocks of dominantly lava facies are preserved within the Khizovaara sequence.

The majority of collected samples shows a mineral assemblage of hornblende-chlorite-plagioclase \pm quartz indicative of medium-grade regional metamorphism. However the samples of boninitic affinity display an unusual mineral assemblage which can be termed as staurolite-bearing amphibolite. The petrography and mineral chemistry of the samples studied by electron probe is summarized in Table 1. As the data clearly suggest, rocks of bulk low-Ti high-Mg tholeiitic compositions are characterized by a plagioclase- and staurolite-free assemblage whereas more evolved rocks exhibit plagioclase-, staurolite- and staurolite-garnet-bearing parageneses. It is significant also that both plagioclase and amphibole compositions are mostly heterogeneous (Table 2). The hornblende (Hbl) and the tschermakitic hornblende (Hbl^{Ts}) are distinctly distinguished chemically by concentrations of Al_2O_3 . Microprobe profiles across plagioclases show their compositional variability from anorthite (Pl^{An}) in cores to andesine (Pl) in rims. Notice that the plagioclase in

Table 1. Mineral assemblages of the boninite series metavolcanics studied by microprobe

Sample	X_{Fe}^{Rock}	Main rock-forming minerals	Opaques
H-333	0.282	Hbl, Cum, Chl	
H-334	0.312	Hbl, Pl, Qtz	
H-326	0.349	Hbl, Chl, Pl, Qtz, Cal	
H-321	0.375	St, Hbl, Chl, Pl, Qtz	Ilm
H-335	0.388	St, Cum, (Ged), Hbl, Chl, Pl, Qtz, (Mica)	Rt, Ilm, Prt, Pnt
H-332	0.381	Grt, St, Cum, (Ged, Hbl), Chl, Pl, Qtz, Ky	Rt, Prt, Pnt, Cpy

Notes: X_{Fe}^{Rock} = molecular ration of Fe/(Fe + Mg). Chemical rock compositions are listed in Table 3. Mineral abbreviations are after Kretz (1983). Mica, K-Ca di-octahedral mica. Minerals in trace constituted are shown in parenthesis.

the paragenesis with staurolite is unzoned anorthite ($An_{0.947}$). Most staurolite and garnet grains are homogeneous, although a limited amount of retrograde zoning is revealed on some garnet rims compared to cores. The above data on zoning of minerals coupled together with their textural patterns suggests that at least two distinct metamorphic episodes (M_1 and M_2 , respectively) formed the observed mineral assemblages of the Khizovaara boninite series.

Staurolite is commonly thought of as a mineral indicative of metapelitic rocks. Recently the possibility of staurolite equilibriums in amphibolites has been theoretically proven by Arnold et al. (2000). Moscovchenko and Turchenko (1975) first discovered and described unusual staurolite-bearing amphibolites in the Iringora Structure. Then Fed'kin (1975) made detailed equilibrium studies of these rocks and assessed their geothermobarometry. However, until now, the origin and significance of these unusual St-bearing amphibolites remained unclear.

Staurolite in the Khizovaara metamorphosed boninites occurs as subhedral grains within a chlorite-amphibole matrix (Fig. 5). It commonly displays resorption relationships with anorthitic plagioclase, and in many examples almost enclosed by the latter (Figs. 5d, e). Fine-grained inclusions of rutile and quartz are also characteristic of the staurolite grains. Apparent equilibrium textures among garnet and staurolite (Fig. 5a), staurolite and rutile, and intergrowths of rutile and gedrite (Fig. 5c) suggest that the all these minerals plus the high-alumina hornblende formed in response to an early metamorphic event (M_1). Relationships between staurolite and kyanite remain ambiguous because they rarely occur in close proximity (Fig. 5b). However the kyanite is commonly replaced by the M_2 -stage chlorite. This in turn suggests that the kyanite may have formed in response to the M_1 event.

In order to decipher a multi-stage metamorphic history of Khizovaara boninite series it is useful to compare the available data on mineral and whole rock chemistry. For this purpose we have plotted both the whole rock compositions of the boninite series and the chemical compositions of the minerals obtained by microprobe technique on both AFM and CFM ternary diagrams (Fig. 6). The model composition of the tholeiite used in the theoretical approach of Arnold et al. (2000) is also shown for reference. As can be seen

Table 2. Representative electron probe average analyses of minerals of the Khizovaara staurolite-bearing metaboninites

Sample Mineral n	H-321					H-335					
	St 3	Hbl 4	Hbl ^{Ts} 3	Chl 2	Pl Rim to Hbl	Pt ^{An} Rim to St	St 5	Hbl 3	Hbl ^{Ts} 4	Cum Rim to Pl	Chl 2
SiO ₂	27.97	46.20	43.52	26.72	57.42	44.58	28.77	46.33	45.34	54.38	25.90
TiO ₂	0.63	0.55	0.44	0.05	0.26	0.01	0.87	0.42	0.38	0.06	0.16
Al ₂ O ₃	52.12	12.15	14.74	21.56	27.05	35.33	52.14	13.68	15.74	1.00	20.73
Cr ₂ O ₃	1.80	0.27	0.49	0.32	0.00	0.16	1.27	0.59	0.52	0	0.49
FeO*	11.63	12.41	12.73	17.75	0.54	0.14	13.07	12.48	12.01	19.46	17.53
MnO	0.32	0.32	0.22	0.13	0	0.06	0.22	0.15	0.18	0.55	0.01
MgO	2.16	12.62	11.09	21.24	0	0	2.30	12.37	11.76	20.08	20.12
CaO	0.06	10.87	10.96	0.06	8.84	18.60	0.03	10.88	10.85	0.78	0.08
Na ₂ O	0	1.36	1.34	0	6.58	0.53	0.33	1.03	1.15	0.01	0.09
K ₂ O	0	0.15	0.23	0	0.04	0.06	0.01	0.08	0.08	0	0
ZnO	1.02	0	0	0	0	0	0	0	0	0	0
Total	97.71	96.90	95.77	87.84	100.74	99.48	99.00	98.00	98.00	96.32	85.11
Si	3.979	6.744	6.462	2.697	2.561	2.068	4.038	6.665	6.509	7.909	2.704
Al ^{IV}	-	1.256	1.538	1.303	1.422	1.931	-	1.335	1.491	0.091	1.296
Al ^{VI}	8.738	0.835	1.042	1.262	-	-	8.625	0.984	1.173	0.081	1.254
Ti	0.068	0.060	0.049	0.004	0.009	0	0.092	0.046	0.041	0.007	0.013
Cr	0.202	0.031	0.058	0.025	0	0.006	0.141	0.067	0.059	0	0.040
Fe ²⁺	1.384	1.515	1.580	1.498	0.020	0.006	1.534	1.501	1.442	2.367	1.530
Mn	0.039	0.040	0.028	0.011	0	0.003	0.026	0.018	0.022	0.068	0.001
Mg	0.458	2.745	2.455	3.196	0	0	0.481	2.652	2.517	4.353	3.131
Ca	0.010	1.700	1.743	0.007	0.422	0.924	0.004	1.678	1.669	0.122	0.009
Na	0	0.385	0.387	0	0.569	0.047	0.090	0.287	0.320	0.003	0.018
K	0	0.029	0.044	0	0.003	0.004	0.002	0.014	0.014	0	0
Zn	0.107	0	0	0	0	0	0	0	0	0	0
Cations	14.984	15.341	15.385	10.004	5.005	4.989	15.033	15.247	15.256	15.000	9.997
X	0.751	0.356	0.392	0.319	0.425	0.947	0.761	0.361	0.364	0.352	0.328

(continued on next page)

Table 2. (Continued)

Sample	H-332										
	Mineral	Grt ^{Alm} Rim to Qtz	Grt	St	Hbl	Cum Rim to Pl	Ged	Chl	Pl ^{An} Core	Pl	Ky
<i>n</i>	8	10	Core	Core	Core	Core	Core	Core	Core	4	3
SiO ₂	37.84	28.32	43.00	55.21	51.26	26.80	45.87	56.71	37.60		
TiO ₂	0	0.77	0.23	0.01	0.18	0.08	0.12	0.03	0.04		
Al ₂ O ₃	20.49	51.81	16.69	0.99	5.42	22.22	33.27	26.25	60.88		
Cr ₂ O ₃	0.11	1.20	0.33	0.20	0.25	0.68	0.02	0.08	0.73		
FeO*	32.53	12.51	11.51	19.86	18.88	13.23	0.32	0.27	0.23		
MnO	1.71	0.08	0.12	0.22	0.21	0.04	0.07	0.02	0.03		
MgO	4.34	2.88	11.34	21.29	19.68	23.72	0	0	0		
CaO	2.56	0.03	10.47	0.30	0.40	0	17.35	8.88	0.02		
Na ₂ O	0	0.12	1.31	0.11	0.41	0	1.45	6.49	0		
K ₂ O	0	0.02	0.26	0.01	0	0.04	0.03	0.05	0		
Total	99.59	97.74	95.26	98.21	96.69	86.80	98.50	98.78	99.52		
Si	3.029	4.014	6.359	7.868	7.425	2.674	2.145	2.577	1.022		
Al ^{IV}	-	0.007	1.641	0.132	0.575	1.326	1.833	1.406	-		
Al ^{VI}	1.933	8.637	1.269	0.035	0.350	1.473	-	-	1.950		
Ti	0	0.082	0.026	0.001	0.020	0.006	0.004	0.001	0.001		
Cr	0.007	0.134	0.038	0.022	0.028	0.054	0.001	0.003	0.016		
Fe ²⁺	2.177	1.483	1.424	2.366	2.287	1.104	0.013	0.010	0.005		
Mn	0.116	0.009	0.015	0.027	0.025	0.003	0.003	0.001	0.001		
Mg	0.518	0.609	2.500	4.523	4.249	3.529	0	0	0		
Ca	0.220	0.005	1.658	0.046	0.062	0	0.869	0.432	0.001		
Na	0	0.033	0.375	0.031	0.114	0	0.131	0.572	0		
K	0	0.002	0.049	0.001	0	0.005	0.002	0.003	0		
Cations	8.001	15.010	15.353	15.052	15.136	9.988	5.000	5.005	2.995		
X	0.808	0.709	0.363	0.343	0.350	0.238	0.867	0.429	-		

Notes: *n*, numbers of analyses; X = Ca/(Ca + Na + K) for plagioclase and X = Fe/(Fe + Mg) for Fe-Mg minerals. Mineral formulae are calculated on oxygen basis: 14 (chlorite), 12 (garnet), 23.5 (staurolite), 23 (amphiboles), 8 (plagioclase) and 5 (kyanite).

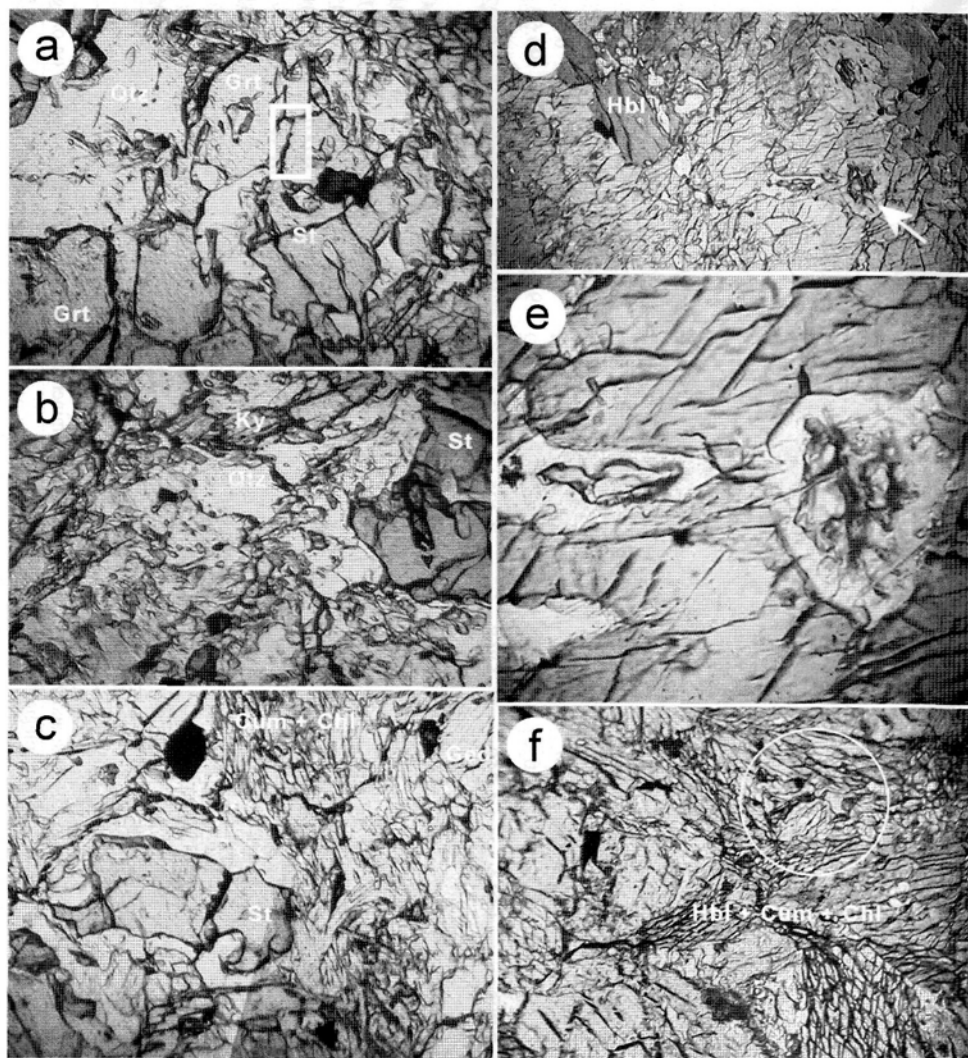


Fig. 5. Microphotographs of Khizovaara St-bearing amphibolites (metaboninites) in the samples H-332 (a–c), H-321 (d–e) and H-335 (f) illustrating textural patterns of the first and second stage mineral assemblages. (a) Boxed area marks a direct contact between Grt and St; note also inclusions of rutile (dark grey) and quartz (light grey) in staurolite. (b) Relationship between St and Ky. (c) Textural patterns of M_1 assemblage (St-Pl^{An}-Ged) and M_2 assemblage (Cum-Chl). (d) Relics of St-Pl^{An} assemblage within the amphibole matrix. (e) 3 times enlarged part of microphotograph (d). (f) Encircled area marks small relics of St-Pl^{An} assemblage. Open nicols. Typical width of microphotograph field is about 1 mm.

from Fig. 6a, the model composition (composition A from the Table 2 of Arnold et al., 2000) fits the neighbourhood of the whole rock trend of Khizovaara boninite series.

Fig. 6b illustrates a good accordance between the whole rock compositions and the mineral chemistry. The major element composition of the sample H-333 plotted on the molecular normative FeO-MgO-CaO-Al₂O₃ tetrahedron falls on the same plane that characterizes the chemical compositions of the homogeneous mineral phases. Because the sample H-333 represents a paragenesis of the least ferruginous minerals, in shifting a bulk rock composition towards the M apex the given mineral assemblage will be kept, but mineral phases will be consistently reduced in iron content. The observed textural features indicate the second-stage (M₂) formation of the Hbl-Cum-Chl assemblage (Fig. 5f).

Some St-free samples occupy the same locus on the AFM/CFM diagrams as St-bearing ones (Sample H-326, Table 1, Figs. 6a, c). This can be explained by a complete replacement of staurolite by later mineral phases. The locus of the mineral chemistry and whole-rock composition points on Fig. 6c suggest that a first-stage assemblage included a mineral equilibrium of tschermackitic hornblende, anorthite and some putative Ca-free amphibole (gedrite). Hereinafter, these were partly replaced by a second-stage mineral assemblage involving chlorite, hornblende with lower Al contents and more sodic plagioclase (Table 2) as compared with the primary metamorphic minerals. It is of interest that a transformation of the M₁ assemblage was accompanied by an emergence of calcite that forms inclusions within the secondary-stage hornblende. This suggests that the bulk alkalinity of the boninite series rocks was almost unmodified. Thus we can infer an isochemical character of the second-stage metamorphism.

A series of compatibility diagrams to illustrate the mineral parageneses for St-bearing samples (= strictly boninitic in a chemical composition) of the first- and second-stage metamorphic episodes is shown on Figs. 6d-f. It should be particularly emphasized that the mineral parageneses of sample H-332 represents a boninitic dacite in chemical composition (Fig. 6f). The seven-mineral assemblage (St-Grt-Hbl-Hbl^{Ts}-Pl-Ky-Qtz) is univariant in the NCFMASH system that has been used by Arnold et al. (2000) to constraint thermodynamic fields of staurolite stability in staurolite-bearing amphibolites. It thus appears that across the thin section studied there are slight variations of the mineral chemical compositions that have given rise to a formation of several divariant mineral assemblages. For instance, in the sample H-332 the staurolite is the most rich in magnesium (Table 2). According to a petrogenetic grid of NCFMASH system (see Fig. 3 from Arnold et al., 2000) a divariant assemblage of St-Grt-Hbl-Hbl^{Ts}-Pl-Qtz is stable within the kyanite field in a range of 620–650 °C at pressure of 6.4–7.8 kbar.

To constrain T-conditions under which the observed two-stage mineral assemblages were formed we tried to use a version of the Hbl-Pl geothermometer (Holland and Blundy, 1994). However due to a high rate of anorthitic end-member in the first-stage plagioclase a majority of the analyzed samples shows unrealistically high elevated temperatures. Equilibrium study on the St-free sample H-334 has shown two distinct groups of hornblende having the Al₂O₃ contents of 14.6 and 11.6 wt% which are associated with two distinct groups of plagioclase having the anorthite mole fractions of 0.688 and 0.419. Taking into account the pressure determination of about 6 kbar obtained earlier by Fed'kin (1975),

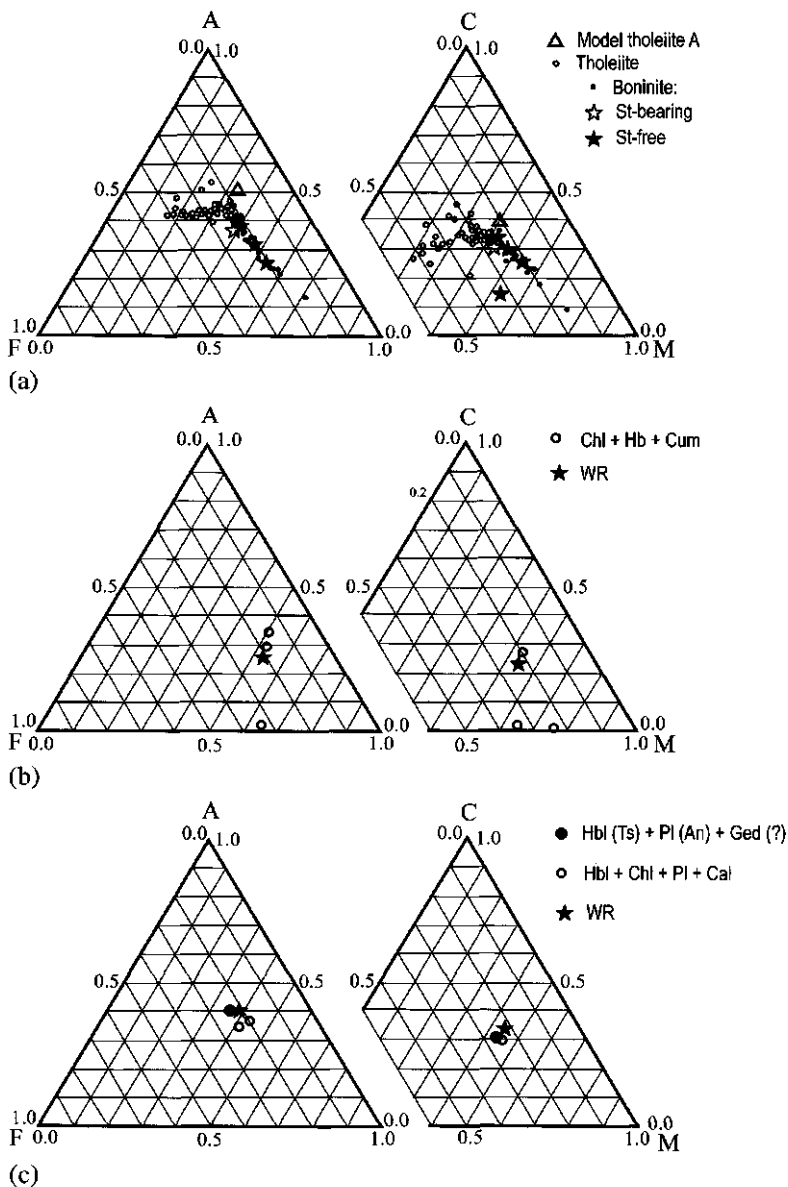


Fig. 6. Series of ternary diagrams illustrating a compatibility exit between major element chemistries of the observed mineral assemblages (\pm quartz) of and available data on the whole rock compositions. (a) Overall tholeiitic trend of Khizovaara boninite series. (b, c) Compatibility diagrams for the both Pl and St free assemblage (b) and the St-free assemblage (c). (d, f) Phase diagrams for St-bearing assemblages. For detail see explanation in the text. Symbols are: M_1 , mineral assemblage; M_2 , mineral assemblage.

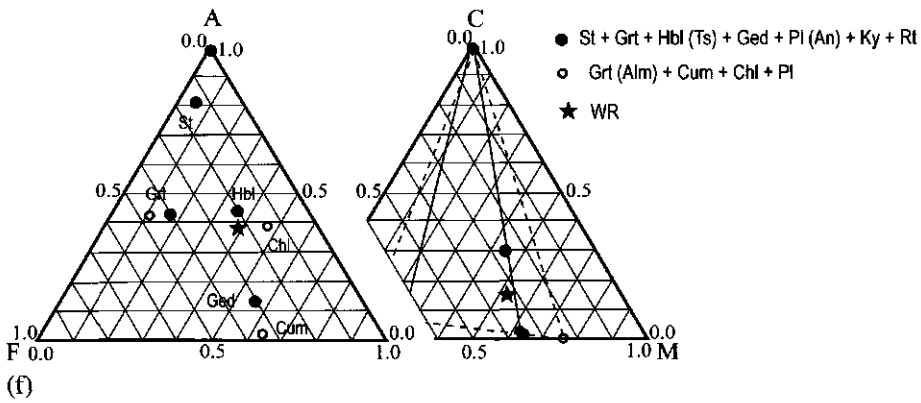
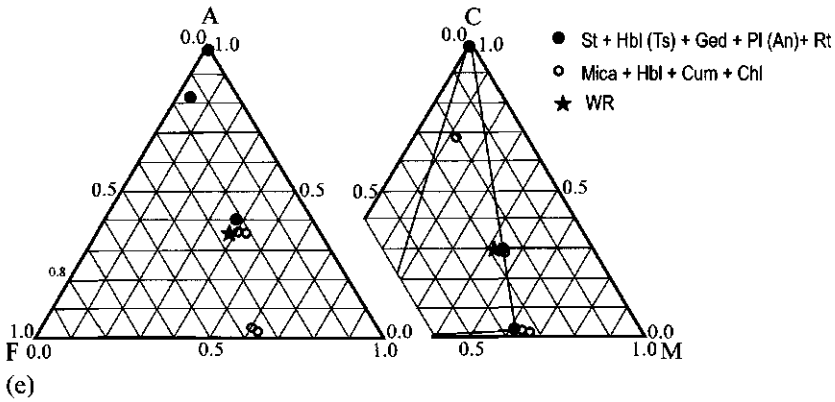
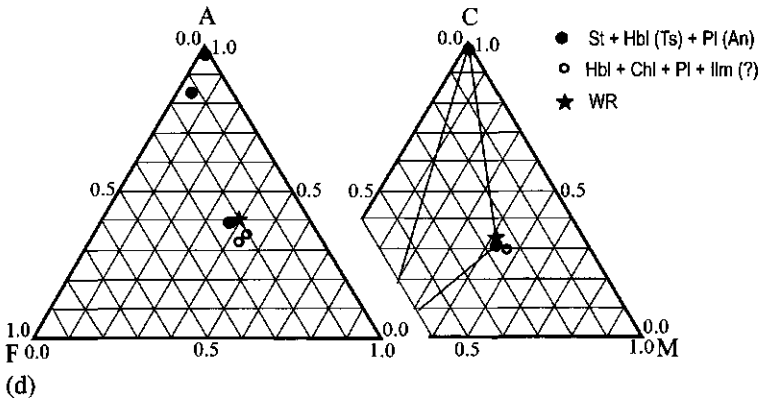


Fig. 6. (Continued.)

these two groups of parageneses correspond to the temperatures of 667 and 579 °C for M_1 and M_2 metamorphic episodes, respectively. In the St-bearing sample H-321 the compositions of the second-stage paragenesis Hbl + Pl (see Table 2) constraint a T-parameter for the M_2 metamorphism as being as high as 598 °C.

Only one sample (H-332) is suitable to use as a staurolite-garnet geothermometer. The different thermodynamic models of staurolite-garnet equilibrium show nearly identical values of M_1 temperature: 692 °C (Perchuk, 1989), 670 °C (Fed'kin and Aranovich, 1990) and 726 °C (Koch-Müller, 1997). These are in a good accordance with the above results of Hbl-Pl thermometry.

It worth noting that the variability in Al content of hornblende mentioned above was detected throughout the analyzed samples. This obviously suggests that the distinct hornblendes, i.e., Hbl and Hbl^{Ts}, were formed subsequently during two metamorphic events that clearly differed in P-T conditions. Nevertheless, as has been argued by Stein and Dietl (2001), an absence of mineral phases to stabilize a hornblende chemical composition precludes using the Al-in-hornblende geobarometer. The same sample H-332 is suitable only to apply the garnet-plagioclase-kyanite-quartz paragenesis (Table 2) for assessing metamorphic pressures by using the model of Newton and Haselton (1981) modified by Koziol and Newton (1989). Allowing for kyanite equilibrium both in the M_1 and M_2 stages, the compositions of garnet and plagioclase appropriate to these stages yield the pressure values of 7.6 and 6.1 kbar for the M_1 and M_2 temperatures of 670 and 580 °C, respectively.

In summary the above P-T values constraining the two distinct tectonothermal events to have formed the Khizovaara metamorphosed boninite series are in agreement with the available structural and isotope-geochronological data. The first-stage mineral assemblages indicative of Barrovian-type metamorphism were developed in response to a Neoproterozoic orogenic/accretionary event between 2.8 and 2.7 Ga. The second-stage mineral assemblages of moderate pressure metamorphism were formed in the Paleoproterozoic during the Svecofennian tectonothermal reworking at 1.9–1.75 Ga ago as determined by U-Pb dating of titanites (Bibikova et al., 2001).

2.4. Iringora Structure

The Iringora Structure is located about 100 km NW of the Khizovaara Structure. It is composed dominantly of the same lithotectonic assemblage that occurs within the latter, except for the Khizovaara's Northern andesite units. Here we have found the same boninite series displaying an ophiolite-like pseudostratigraphy unique to the Archean.

The Iringora ophiolite-like sequence occurs within a thrust stack gently plunging to the N-NE. This stack preserves several imbricate slices of c. 2.8 Ga mafic volcanic rocks, including both the boninite series and the upper tholeiites of MORB-like affinity, overthrust onto the tectonically juxtaposed complex of arc-derived acid-felsic volcanics and siliciclastic turbidites (Fig. 7). Thus, the above mentioned complex of the arc-trench/forearc system represents an autochthon for the Iringora ophiolite-like sequence. Although the entire Iringora sequence has been intensely deformed and metamorphosed, primary igneous, volcanic and sedimentary features fortunately are locally well preserved. The best

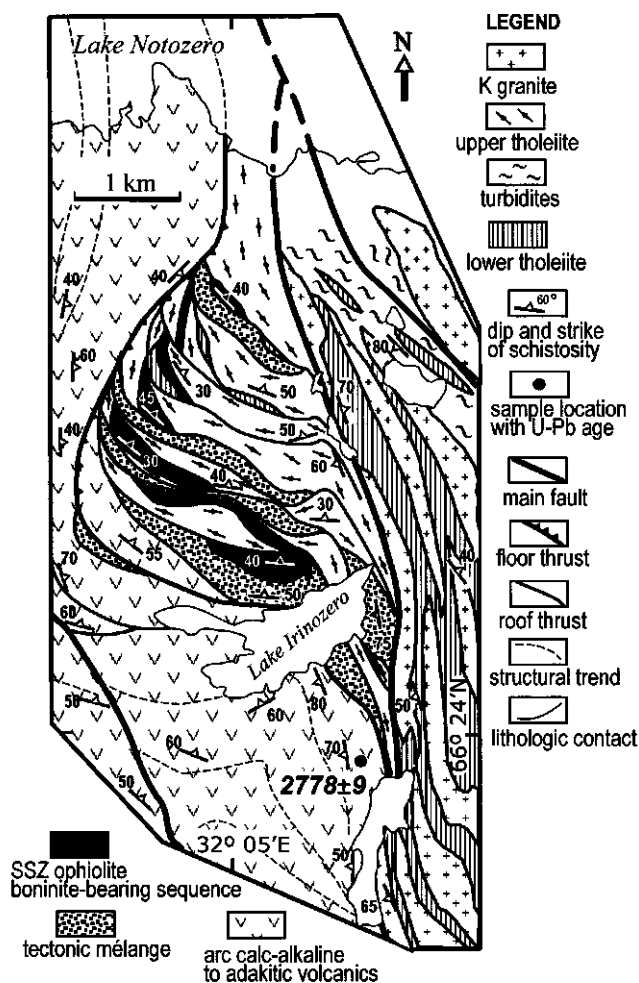


Fig. 7. Geological map of the Iringora Structure.

preserved fragment of the ophiolite-like sequence occurs along the north shore of Lake Irinozero where not only gabbroic and lava units, but also remnants of a sheeted dike complex, including half dikes and cusps of dikes, i.e., a transition of dikes into the lava unit, are exposed. Moreover, at the base of the ophiolitic nappe there is a complex of tectonic mélangé metamorphosed in the mode of a metamorphic sole.

Boninite-bearing ophiolite-like assemblage. The structurally lowermost slice of the Iringora ophiolite-sequence consists of an up to 500 m thick pile of sheeted dikes and well-preserved lava complexes overthrust, in turn, by slices of the ophiolitic gabbro and

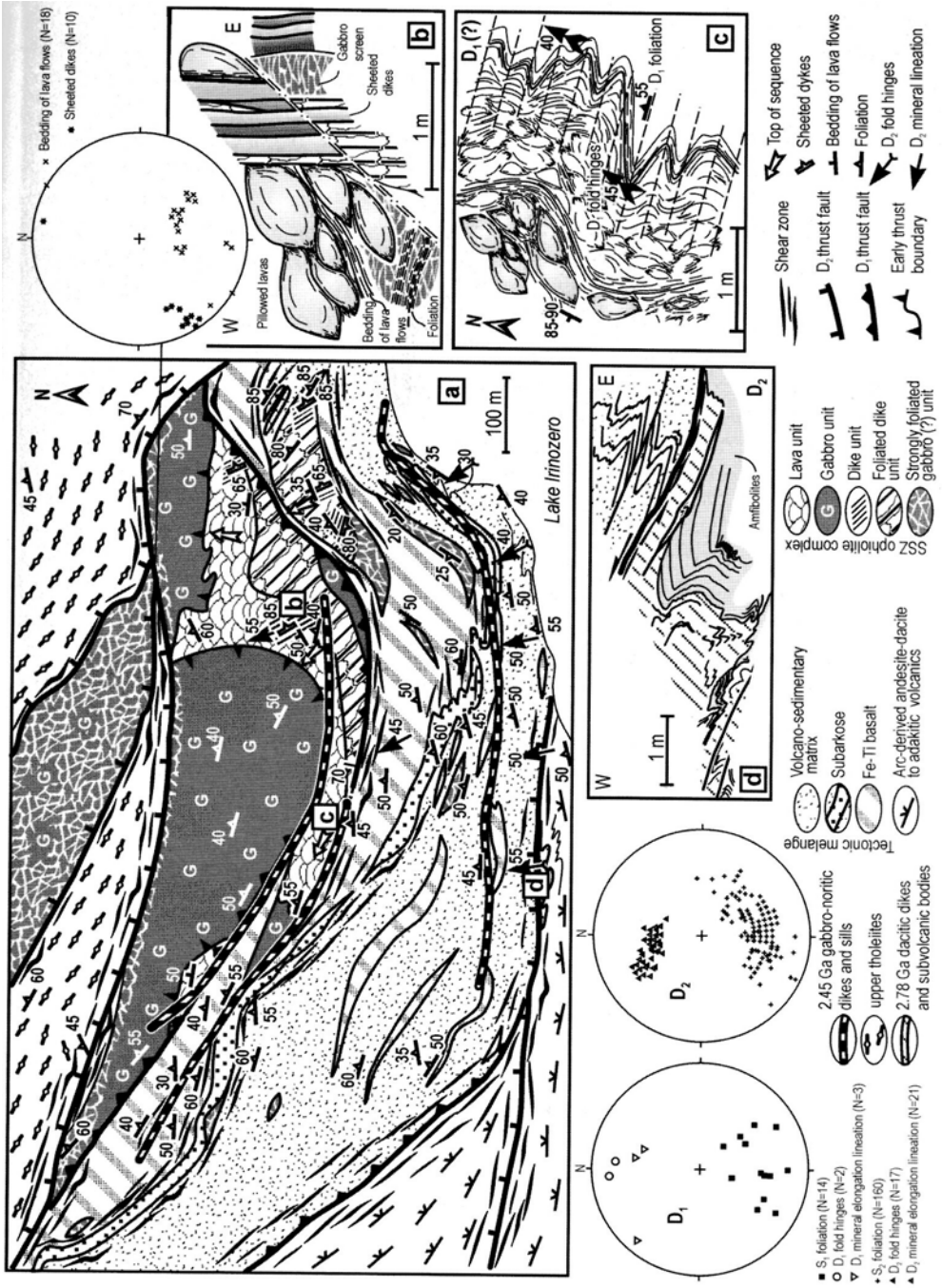
the upper tholeiites (Fig. 8). Owing to the prominent volcanic textures, the lava unit is the most easily identified.

Lava unit. Although the thickness of the lava units along the north shore of Lake Irinozero is no more than 100–150 m, the preservation of primary volcanic textures is striking. The lava unit comprises dominantly both pillowed and massive flows. Pillows are a fairly uniform size commonly nearly 40–50 cm in two-dimensional exposures, while locally larger (up to 1 m) as well as smaller pillowed textures occur. Individual massive flows are from 2 to 3 m in thickness. They are visibly outlined by a cumulate zone at the bottom and by autobreccia at the top of each flow. Yet another striking feature of the lava unit is a preservation of mafic pillow breccia and pillow clusters. The breccia consists of fragments of pillow lava in a finer-grained, fragmental, and shard-rich matrix, displaying in some cases the classic pattern of hyaloclastic breccia. In such cases the clasts are commonly between 5 and 20 cm in diameter. This indicates that the cooling units experienced contact with water and were erupted in a submarine environment. Moreover, the whole Iringora lava unit displays no evidence for interflow sediments or visible vesicular textured pillows suggesting that it could have been erupted in a deep-water environment. Aside from the uniquely preserved primary volcanic textures, the rocks of the Iringora lava unit are identical in their petrography and mineral compositions to the Khizovaara boninite series.

Dyke unit. Uniformly layered medium- to fine-grained rocks underlying the lava unit are interpreted as a dense swarm of tholeiitic and boninitic dikes, i.e., a sheeted dike complex. The latter differs from the foliated gabbro in dike width (average 40–50 cm) and texture displaying in some places evidence for screens of earlier crust. In the field occurrence the largest portion of this unit appears somewhat different from either the lava unit or the gabbro unit. However, there are a few outcrops within the unit where preserved textural features displaying a sheeted dike affinity do occur. A single outcrop exhibits occurrences of preserved chilled margins indicating the development of dike-within-dike relationships (Fig. 9). Furthermore, the transition from sheeted dikes to volcanics is also preserved in a few localities where the sheeted dikes cut roughly perpendicular the overlying volcanics (Figs. 8b, 10). It is crucial also that rocks of boninitic composition are found both in the lava and in the dike units.

Gabbro unit. Medium- to coarse-grained, compositionally layered mafic rocks of the Iringora sequence are interpreted as a gabbro unit, which appears to be the deepest level of ophiolite exposed. The detailed mapping of the Iringora ophiolite-like sequence has shown that the gabbro unit occurs structurally higher than the lava unit and was overthrust onto the latter. Only a few small bodies of gabbro are exposed along with the dyke unit possibly representing screens of earlier crust. Due to a strong schistosity, primary gabbro textures such as modally graded layers are preserved in only a few localities of low strain. The principal schistosity (S_2) is sub-parallel to compositional layering and is interpreted

Fig. 8. Detailed geological map of the north shore of Lake Irinozero (a), equal area, lower hemisphere stereographic projections for poles to the D_1 and D_2 fold axial planes and outcrop sketches (b–d) showing some principal fabric elements of the Iringora ophiolitic sequence.



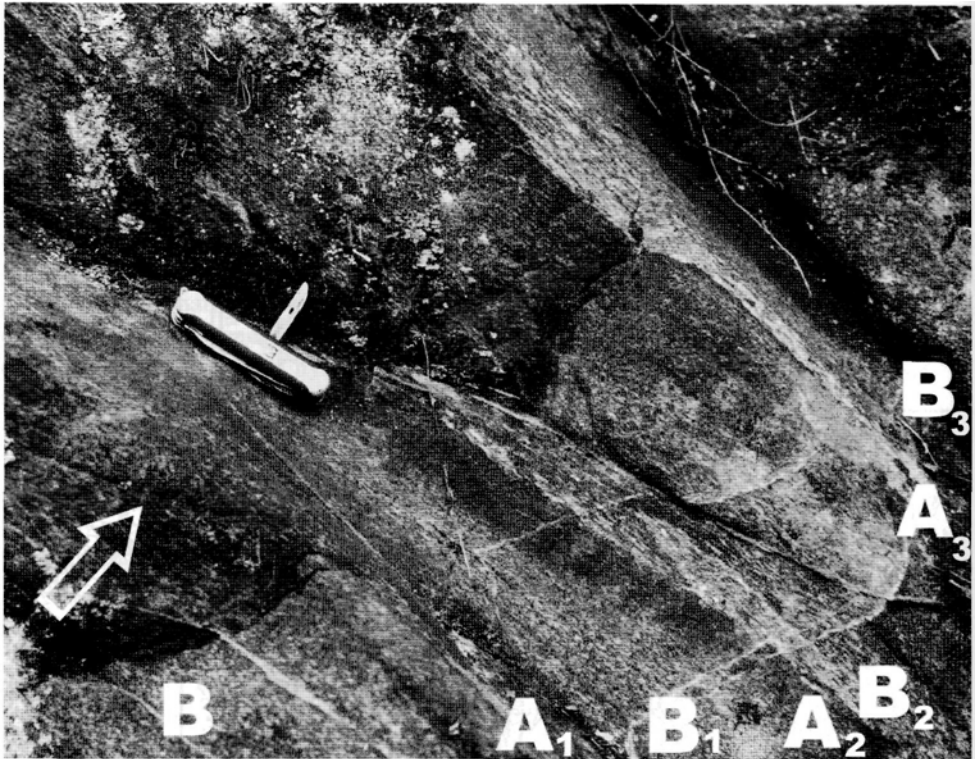


Fig. 9. Field photograph of the Iringora sheeted dike complex with asymmetric chilled margins of the same polarity indicating dike-within-dike relationships. The arrow shows the spreading direction. (A) Chilled margins and (B) central parts of the dikes.

as transposition of primary layering into the S_2 plane during the main Neoproterozoic (D_2) deformation and metamorphism phase. Although there is no direct evidence for a 'normal' ophiolitic relationship between the gabbro unit and the presumably overlying sheeted dike complex, it is crucial that several observed dikes were mapped to be intrusive into the gabbro unit in some places. Coupled together with the compositional features of the gabbro unit, this may imply that initially the latter was directly related to the overlying dike and lava units. The available geochemical data on the Iringora gabbro unit suggest without doubt that it has the same parent magmas as both the volcanic and dike unit.

The dike unit is underlain by tectonic melange (Fig. 8). The basal contact represents a décollement zone, or a floor thrust in terms of the geometry of duplex structures (Moores and Twiss, 1995). The gabbro unit occurs structurally higher, together with the upper tholeiites in roof thrusts. This, in turn, may imply that the décollement zone along which the ophiolitic rocks were emplaced may have propagated toward the top of the ophiolitic sequence leading to the development of the imbricate stack during an accretionary event.

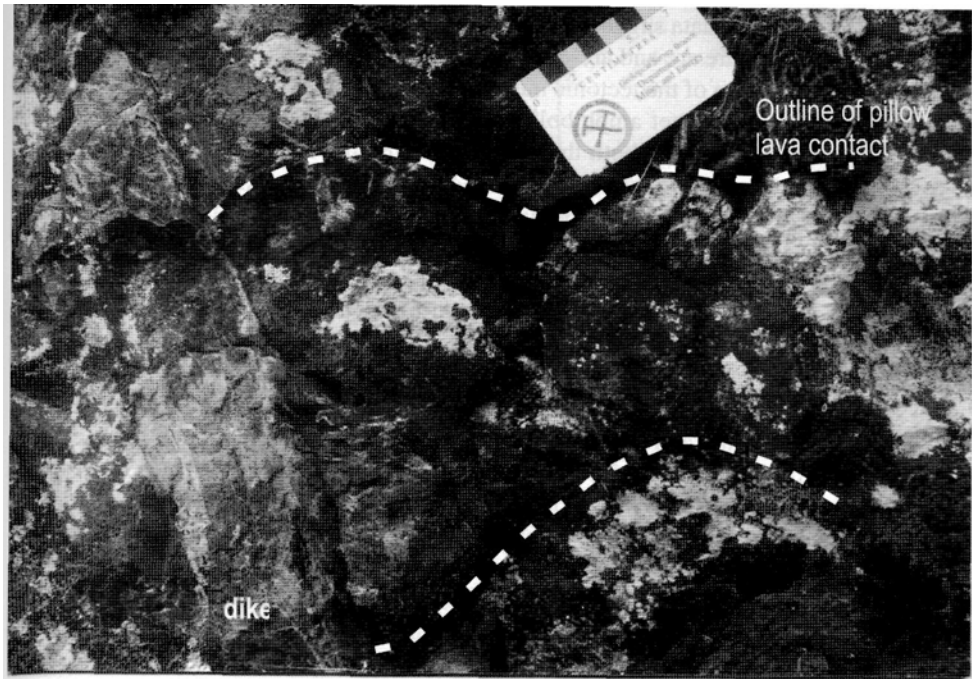


Fig. 10. Field photograph of the preserved transition zone between the Iringora dike and lava units. It is clearly visible that the dike cuts roughly perpendicular the volcanic pillow. Light patches on the rock exposure surface are outgrowths of lichen.

Tectonic mélangé and metamorphic sole. At the base of the ophiolitic nappe there is a sheared chaotic rock unit without discernible stratification, of up to 300 m thickness, interpreted as a tectonic melange. The tectonic melange consists of internally fragmented rock bodies containing a mixture of native (i.e., rocks of the boninite series) and exotic (Fe-Ti basalts) blocks in a volcano-sedimentary matrix. In contrast to the Khizovaara sequence, along the entire Iringora sequence the Fe-Ti basalts occur only as 'facoids' within the tectonic melange. Native blocks are represented by strongly recrystallized coarse-grained low-Ti high-Mg amphibolites. Blocks range in size from a few millimeters to, at least, several tens of meters. Because of intense shortening and shearing, blocks tend to be flattened and lens-shaped. In many cases exotic blocks truncate the ophiolitic blocks and vice versa. The propagation of shear zones into the lensoidal blocks resulted in further internal fragmentation, chipping off smaller fragments (Fig. 8d). The matrix is composed of petrographically diverse garnet-, staurolite-, kyanite-, and amphibole-bearing micaschists with lenses of subarkosic sandstone and rarely carbonaceous schist. At the bottom of the tectonic melange the matrix displays some evidence that it is partially derived from the underlying arc volcanic and volcano-clastic rocks. To the north of the Irinozero lake shore, the matrix grades into less mature red-colored medium- to thick-bedded siliciclastic schists of

turbiditic affinity. These data suggest that the ophiolitic nappe was thrust onto the accreted assemblage of the mature arc and arc-derived trench or forearc slope turbiditic sediments.

The uppermost 100 m of the tectonic mélangé is composed of garnet-staurolite-kyanite-plagioclase schists and garnet amphibolites displaying an otherwise coarse-grained porphyroblastic texture relative to both the overlying ophiolitic and underlying volcanoclastic rocks. It should be noted that such unusual coarse-grained rocks containing high P-T minerals occur only along with the footwall of the ophiolitic nappe. These grade rapidly downward into kyanite-free and medium- to fine-grained rocks. Microprobe studies of these rocks have shown that the core compositions of garnet-biotite-hornblende assemblage record a T-parameter as high as 700 °C. Unfortunately we have still not detected in thin section a suitable mineral paragenesis to assess a P-parameter with accuracy. However a geological position of this coarse-grained assemblage that is unusually rich in kyanite and garnet suggests that it could be developed under high-PT conditions (> 7 kbar, at least, and about 700 °C) all indicative of the metamorphic sole of a thick and hot ophiolitic nappe.

Upper tholeiites. The field appearance and major- and trace geochemistry of the Iringora upper tholeiites show that this unit is the same as that within the Khizovaara Structure. It is composed of pillowed and massive lava flows of basalt to andesitic basalt of MORB affinity accompanied by co-magmatic gabbro sills. The Iringora upper tholeiites occur tectonically both above the lava unit and the gabbro unit of the SSZ ophiolitic sequence, thus implying that an early thrusting event took place during accretion of an arc-trench system and imbrication of the ophiolitic sequence.

Arc-trench assemblage. The southern and western segments of the Iringora Structure are composed predominantly of acid-felsic volcanic and volcanoclastic rocks whereas the NW flank reveals a thick pile of siliciclastic sediments. Farther west and south-west still, two elongated dome-like granodiorite massifs (not shown) are interpreted in terms of major and trace geochemistry as intrusive analogues to the acid-felsic volcanic rocks. Due to large deformational and metamorphic transformations, most parts of the volcanic rocks lost primary textures and are geochemically and mineralogically identifiable as being of calc-alkaline to adakite affinity. The few outcrops of this unit suggest that these originally were eruptive rocks developed as lava flows, tuffs and flow breccias and agglomerates ranging in composition from andesites through dacite to rhyodacites. Among the younger volcanic products, dacitic to rhyodacitic dykes and shallow-level sills are particularly common. Some dykes or small dome-like bodies display silica-rich rhyolitic compositions. In addition, relatively small sill- and dyke-like bodies scattered throughout the arc-derived volcanics are 'normal'-Ti (approximately 1 wt%) and some are high-Al gabbros. Along the contact with the tholeiite-ophiolite imbricate stack the arc volcanics are interlayered with compositionally similar sandstones.

Based both on the field appearance and geochemical characteristics, it seems obvious that the Iringora calc-alkaline volcanics are close analogues of the Khizovaara Southern lithotectonic assemblage. Moreover zircons from a dacite subvolcanic body cutting the Iringora arc volcanics yield a U-Pb discordant age of 2782 ± 9 Ma obtained by conventional method (Fig. 11), i.e., showing within the analytical error the same age as the Khizovaara arc volcanics.

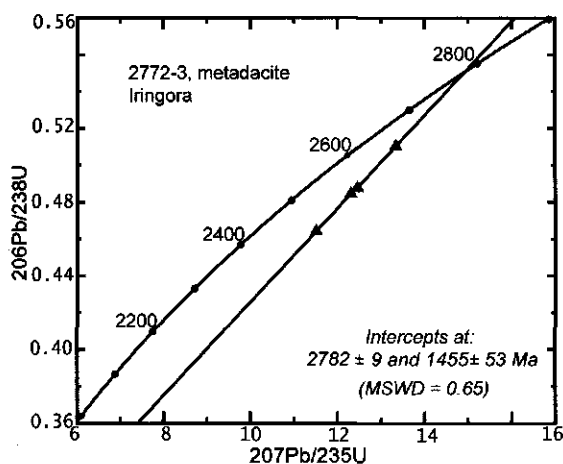


Fig. 11. Concordia diagram showing plots of zircon fractions from the Iringora dacite (sample 2772-3).

Sedimentary rocks occupy the NE flank of the Iringora Structure. They are characteristically red-colored contrasting to the light-grey colored arc volcanics. Although in some cases sedimentary rocks are interbedded with the arc volcanics, the bulk of the thick sedimentary pile occurs as a fault-bounded sedimentary domain. In spite of the fact that primary sedimentary structures such as parallel bedding, cross-bedding, and grading are intensely deformed throughout the domain, their turbiditic affinity is clear. These sedimentary rocks consist mainly of thick- to medium bedded greywacke-mudstone pairs and are characteristic of sediments deposited by turbidity currents. Sandstones tend to be more abundant and thicker than siltstone and shale pairs. Locally preserved features such as grading, sole marks and cut-and-fill structures indicates that many, if not all, sediments are proximal turbidites derived from nearby volcanic highlands and deposited in a forearc/trench slope setting. Volumetrically, greywackes of andesitic and rhyodacitic composition prevail, but basaltic greywackes tend to be more abundant in the upper level of the sedimentary pile. Some turbiditic outcrops show occurrences of relatively thin (20–40 m) slices of amphibolites both of 'normal'-Ti and high-Ti tholeiite compositions which can be interpreted as scraped-off sections of oceanic crust in the Iringora accretionary prism. Geochemically, the 'normal'-Ti amphibolites are similar to the Khizovaara lower tholeiites, whereas the high-Ti amphibolites are akin to the Khizovaara ferro-tholeiitic basalts.

Structural development. The present structural framework of the Iringora greenstones is largely due to an overprinting effect attributed to several subsequent deformational phases developed both in the Neoproterozoic and Paleoproterozoic. In order to decipher the Neoproterozoic structural development, as a first step, we must assess the succession and style of Paleoproterozoic refolding. For this purpose, we have used the data previously attained on the Kukasozero belt (Babarina, 1998) which is located about 15 km W of the Iringora Structure and involves a thick sequence of Paleoproterozoic (Karelian) volcano-

sedimentary rocks. The deformation history of the Paleoproterozoic rocks includes at least two folding stages. During the first stage (D_3), they were affected by northward-trending recumbent folding of eastward-trending vergence and associated thrust faulting. During the second stage (D_4) a regional thrust plane formed. This was reworked into NS-NE-trending upright open folds which, during the progressive contractional deformation, developed along with their antiformal planar axis into the closed tight folds or the fault zones. The latter represent a sort of layer-parallel faulting formed as a result of 'rock squeezing' between the adjacent synformal counterparts (Fig. 12).

With respect to the main Paleoproterozoic deformational patterns, the Neoarchean Iringora sequence occurs within the synformal domain, i.e., within the domain of lower Paleoproterozoic strain. That is the reason that some important primary igneous textures indicating an ophiolitic setting were preserved within the study areas. Two early nappe-style deformational events are documented in the Neoarchean Iringora sequence. Although the largest portion of the Iringora greenstones underwent obviously intense transformation during the D_2 and subsequent Paleoproterozoic D_3 and D_4 deformation phases, nevertheless some unique evidence of the earliest D_1 ophiolitic thrusting is preserved along the northern shore of Irinozero Lake (Figs. 8b, c). The major ophiolite nappe boundary is distinctively marked by the tectonic *mélange* and the metamorphic sole. In addition, the earliest foliations and mineral stretching lineations occasionally appear within the best preserved and primary igneous textured lava unit. The orientation of the D_1 fold hinge and axial planes was modified during the subsequent D_2 deformational phase crucial in development of the Neoarchean structural pattern.

Second-generation structures are dominated by several map-scale ENE to EW trending thrust zones defining a duplex geometry of the entire Iringora ophiolitic sequence. Thrust zones are typically from 0.5 m to few meters thick and are defined by development of mylonitic fabrics indicating intense shearing along thrust boundaries. These imbricate thrusts generate their own minor folds with westward vergence. It should be noted that several thrusts have been identified, but extensive inverted sequences resulting from recumbent folding are not common. These imbricates wrap around Iringora mountain, consisting of relatively thin slices of arc-derived volcanics, tectonic *mélange*, largely dismembered ophiolitic rocks, upper tholeiites and siliciclastic turbidites. Furthermore, syn-tectonic fault-bounded panels of red to pinkish granite were emplaced into the volcanic and volcanoclastic rocks semi-simultaneously with the D_2 deformation phase. Compared to the Paleoproterozoic structural development, the Neoarchean phase was accomplished by progressive west-vergent tectonic transportation leading to a regional shortening, crustal thickening and Barrovian-type metamorphism.

3. GEOCHEMISTRY

Analytical methods. Chemical studies were undertaken on 15 g aliquots from 400 to 500 g of sample, reduced with a jaw crusher and ground twice in a corundum mill. Major elements were determined by XRF on fused glass pellets using a VRA-20R apparatus at

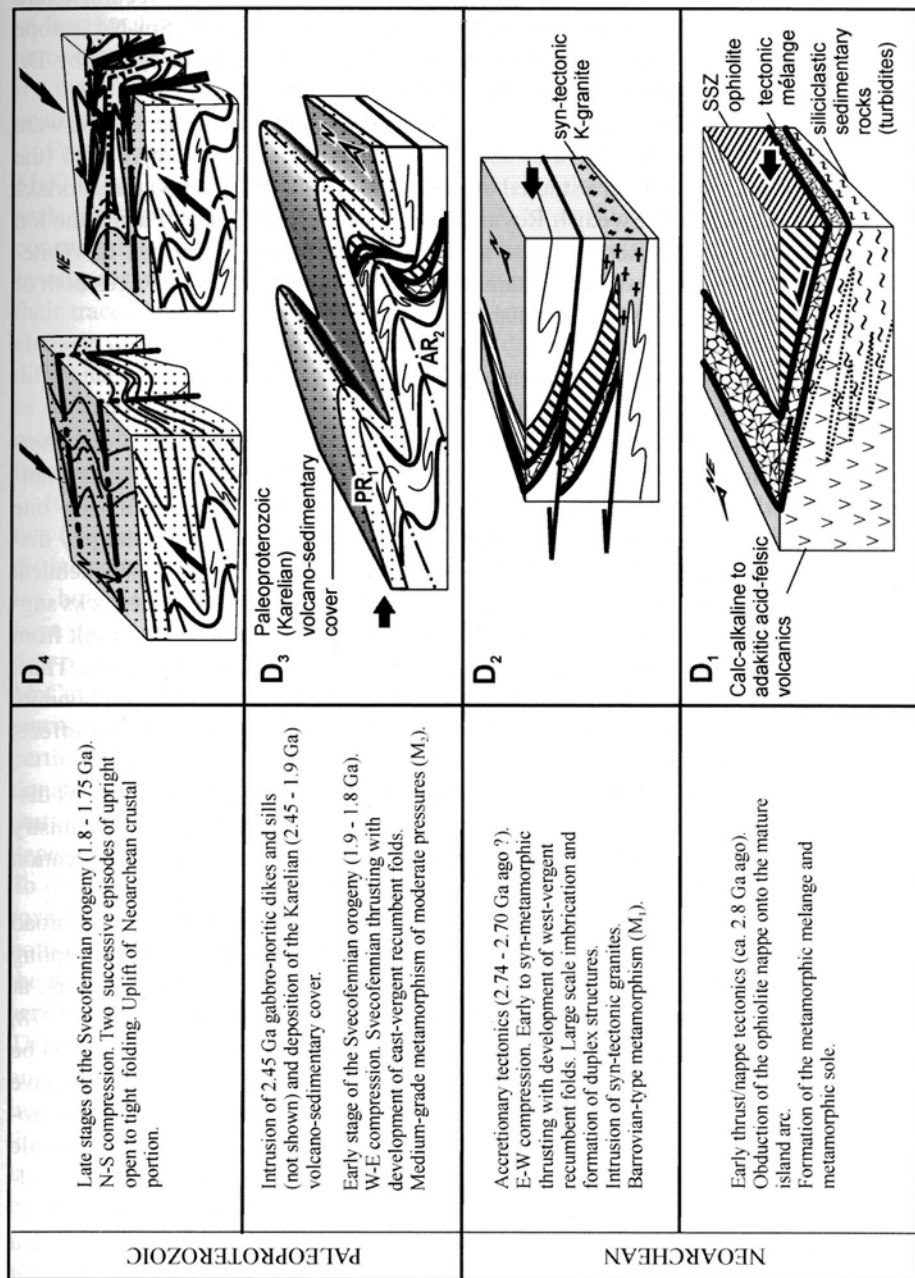


Fig. 12. Summary and sketch of the structural development of the Iringora SSZ ophiolite.

the United Institute of Ecology, Geophysics, and Mineralogy, Novosibirsk, Russia. All Fe is done as Fe_2O_3 . The trace elements were analyzed by inductively coupled plasma spectrometry (ICP-MS) in the Mendeleev Analytical Center, St. Petersburg. Accuracies are estimated as follows: $\sim 2\%$ for major elements, $\sim 5\%$ for trace element. Sm-Nd isotope investigations were carried out at the Max-Planck-Institut für Chemie in Mainz by Dr. I. Puchtel following the technique described by Puchtel et al. (1997).

The procedures used for the conventional U-Pb age determination of the zircons were similar to those described by Bibikova et al. (1996). Zircons from the sample 7/96 (the Khizovaara Northern andesite) were studied at the Isotopic Laboratory of Naturhistoriska Riskmusset in Stockholm (the Swedish Royal Museum of Natural History) using the ion microprobe Cameca 1270 NORDSIM. The analytical procedure is described in Whitehouse et al. (1997). The analytical data obtained to constrain the above U-Pb ages both of Khizovaara and Iringora rocks will be published elsewhere.

3.1. Geochemistry of the Boninite Series and Related Mafic Rocks

Chemical effects of alteration. All analyzed samples have experienced repeated metamorphism and likely prior submarine hydrothermal alteration. Consequently, no primary minerals were preserved in the NKGB sequences. From the sophisticated point of view one could expect that primary igneous compositions of the analyzed rocks were largely disturbed, as well. Of particular interest is the case of metamorphic rocks with geochemical boninitic affinity because the presence of staurolite and quartz along with these rocks suggests excesses of Al, Si over alkalis. Among other reasons this could probably result from a sea-floor hydrothermal alteration that enriched rocks in Mg and removed alkalis. Thus, a major problem in the chemical characterization of the NKGB metamorphosed boninite series and the interpretation of its petrological evolution is to identify and assess the effects of alteration, and to distinguish them from igneous processes.

In order to resolve this problem, as a first step, we sampled rocks from outcrops displaying no evidence for late-stage tectonic fabrics. Then, coherency of the geochemistry was considered in conjunction with detailed petrographic observation for the identification of least altered samples.

Based on a large number of studies in Archean greenstone belts, there is a broad consensus that Al, Ti, the HFS elements (Th, Nb, Ta, Zr, Hf, Y), the REE (excepting Eu) and the transitional elements (Cr, Co, Ni, Sc, V) are relatively immobile during, at least, low-grade metamorphic alteration (e.g., Condie et al., 1977; Sun and Nesbitt, 1978; Ludden et al., 1982; Shervais, 1982). In contrast, Ca, Na, K, Rb, Sr, Ba and Cs could be generally mobile. However, most of the alteration studies for Archean metavolcanics have been done on komatiites and related rocks. Poidevin (1994) has shown that the Paleoproterozoic Bogoin boninites affected by high greenschist metamorphism have kept magmatic affinities for most of the major elements (except Na and perhaps K) whereas their trace element abundances are very similar to recent boninites.

We tried to assess a possible degree of alteration of the NKGB boninite series using a combination of distinct geochemical and petrological approaches. It is worth noticing that

a simple application of Bi-variate diagrams for rocks of boninite series to evaluate possible effects of their post-magmatic alteration faces problems. This can stem from a number of processes involved in their petrogenesis including: melting processes, complex paths of fractional crystallization, different mantle source and metasomatizing components, or some combination of these processes. Despite this complexity, the problem can be resolved if a major- and trace-element dataset is coupled with that from unmetamorphosed possible analogues, as outlined below.

First of all, it needs to be ascertained that the NKGB rocks of boninitic affinity, i.e., $\text{MgO} > 8\%$, $\text{SiO}_2 > 52\%$ and $\text{TiO}_2 < 0.5\%$ (Le Bas, 2000), are not products of large-scale post-magmatic addition of SiO_2 (up to 15%) into the high-Mg and less siliceous counterparts. In comparing the low-Ti tholeiitic and strictly boninitic compositions on the mantle-normalized diagrams, both compositional groups show no marked differences in their trace element patterns (Fig. 13). This suggests the preservation of magmatic trace element values rather than their disturbance due to a post-magmatic silicification. Some differences can be seen for the third group, including that the most evolved rocks occur as remnants of felsic dykes. However the pronounced negative Eu anomalies and some more fractionated LREE compared to the less evolved groups are attributable to a strong fractionation of plagioclase and, perhaps, amphibole.

It should be noted that all the three compositional groups bear the pronounced positive Sr anomalies. This regularity may be of particular interest taking into account two distinct circumstances. On the one hand, Sr is commonly regarded to be mobile during both hydrothermal and metamorphic alteration processes. On the other hand, a large positive Sr anomaly is one of the crucial features for identification of subduction-related volcanics from recent as well as ancient arcs (e.g., Pearce et al., 1984; McCulloch and Gamble, 1991). The recent study on the determination of trace element partition coefficients between garnet, clinopyroxene and hydrous basaltic liquids mostly pertinent to processes in subduction zone has shown that clinopyroxene-dominated fractionation may produce a positive Sr spike in melt from magma without anomalous Sr contents generated in the spinel lherzolite field (Green et al., 2000). This result provides an independent way to assess effects of alterations for Sr and CaO in the NKGB boninite series. To do this, we need to choose two pairs of element ratios mainly controlled by clinopyroxene fractionation. These are $\text{CaO}/\text{Al}_2\text{O}_3$ and Sr/Ce , because Cpx fractionation forces both the removal of CaO relative to Al_2O_3 and the progressive enrichment in Sr relative to the neighbouring MREE. However, it is widely accepted that boninite series compositions are controlled by subsequent crystal/liquid fractionation from a boninite parental magma. The order of crystallization is generally chrome spinel-olivine-both pyroxenes-plagioclase-amphibole-magnetite (e.g., Ohnenstetter and Brown, 1996). If such complexity exists, it is important to isolate more evolved liquids which could be also controlled by crystal fractionation of plagioclase. As shown on the Bi-diagrams (see Figs. 15, 16), the Al_2O_3 content increases until $\text{Mg}\# (= \text{Mg}/(\text{Mg} + \text{Fe}^{2+})) \sim 0.70$, while Fe_2O_3 decreases, reflecting the late crystallization of plagioclase in this series. In the rocks with $\text{Mg}\# < 0.70$ Al_2O_3 decreases rapidly, reflecting the crystallization of clinopyroxene together with plagioclase. Thus, the rocks with $\text{Mg}\# > 0.70$ or $\text{MgO} > \sim 10 \text{ wt}\%$ are included in the further proceeding. Finally,

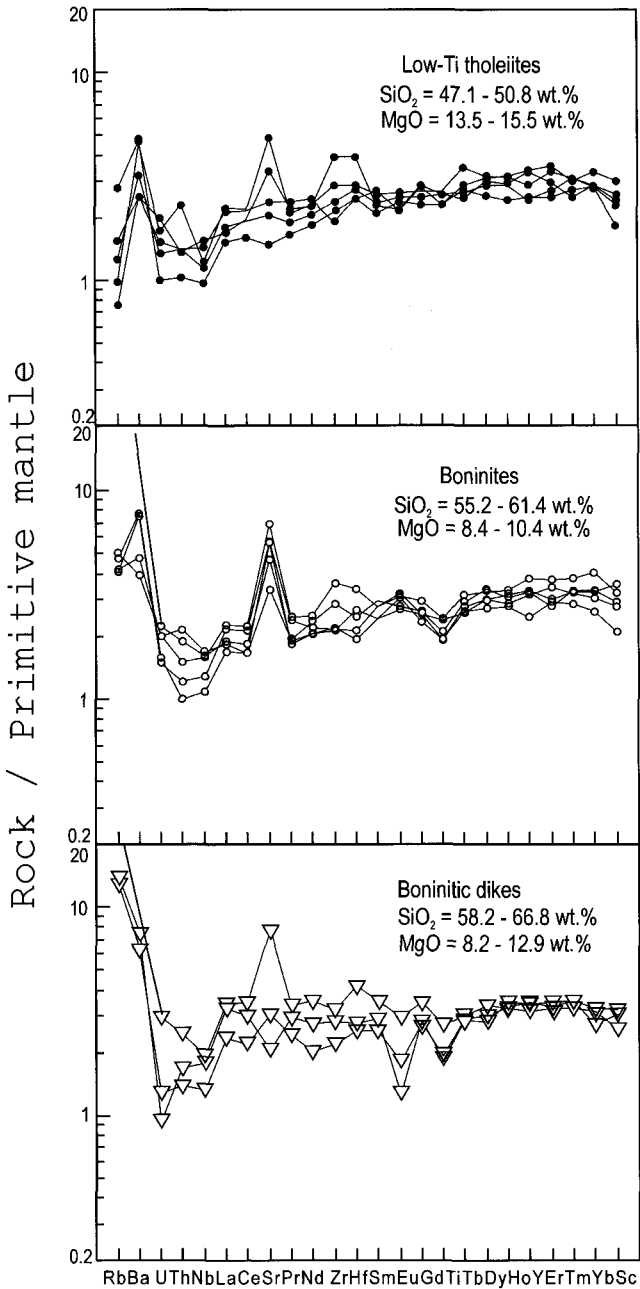


Fig. 13. Trace-element spidergrams for NKGB boninites and low-Ti tholeiite lavas normalized to primitive mantle values of Hofmann (1988).

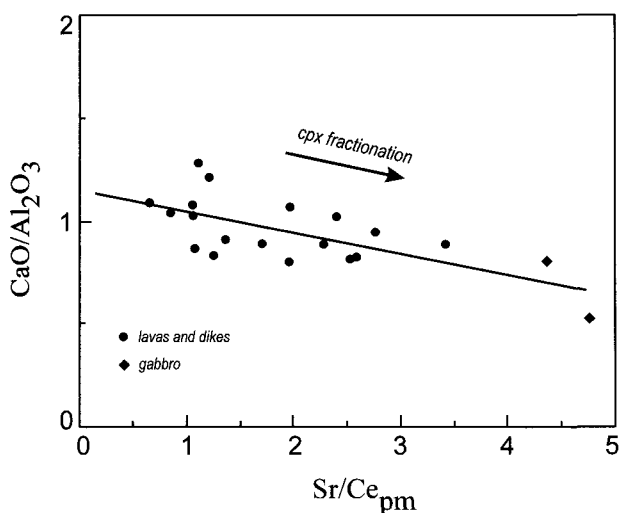


Fig. 14. Plot of $\text{CaO}/\text{Al}_2\text{O}_3$ versus $\text{Sr}/\text{Ce}_{\text{pm}}$ for selected samples in the NKGB boninite series. See explanation in the text.

the plot $\text{CaO}/\text{Al}_2\text{O}_3$ versus $\text{Sr}/\text{Ce}_{\text{pm}}$ demonstrates a good correlation ($r = -0.74$) indicating that the Sr content was mainly controlled by clinopyroxene fractionation (Fig. 14). The two analyzed layered gabbro samples from the Iringora sequence are a good match for the deduced fractionation trend. This, in turn, suggests that the CaO and Sr contents in the analyzed samples essentially reflect their igneous affinities while CaO could be mobile to some extent in those rocks during the sea-floor alteration of the glass. The relative immobility of CaO in boninites series in such process may be because a large fraction of CaO resides in the unaltered groundmass clinopyroxene, rather than in (albitised) plagioclase laths as in the tholeiites (Meffre et al., 1996).

In addition, considering the other evidence pointing toward a boninitic affinity for the NKGB metamorphosed rocks given below, a large post-magmatic alteration for clear resemblance with some unmetamorphosed boninite series in term of most of the major- and trace elements seems incredible. This is not to say that there was no post-magmatic disturbance at all. For example, NaO, K_2O , Ba, Rb, Cs display scatters fields on the plots versus incompatible elements (not shown), that are likely attributable to hydrothermal or metamorphic remobilization.

Fractionation history. Distinctive geological and geochemical characteristics of the NKGB mafic volcanic rocks have permitted a subdivision into four suites (Fig. 3): lower tholeiites, boninite series, Fe-Ti tholeiites and upper tholeiites. TiO_2 coupled with MgO or Mg# values are particularly attractive for individualization of different rock-types. The considerable geochemical diversity between these volcanic suites in terms of their major and trace element compositions is illustrated in Fig. 15, in which the fields of the three late Paleozoic volcanic suites combined into the Koh SSZ ophiolite sequence, New Caledonia

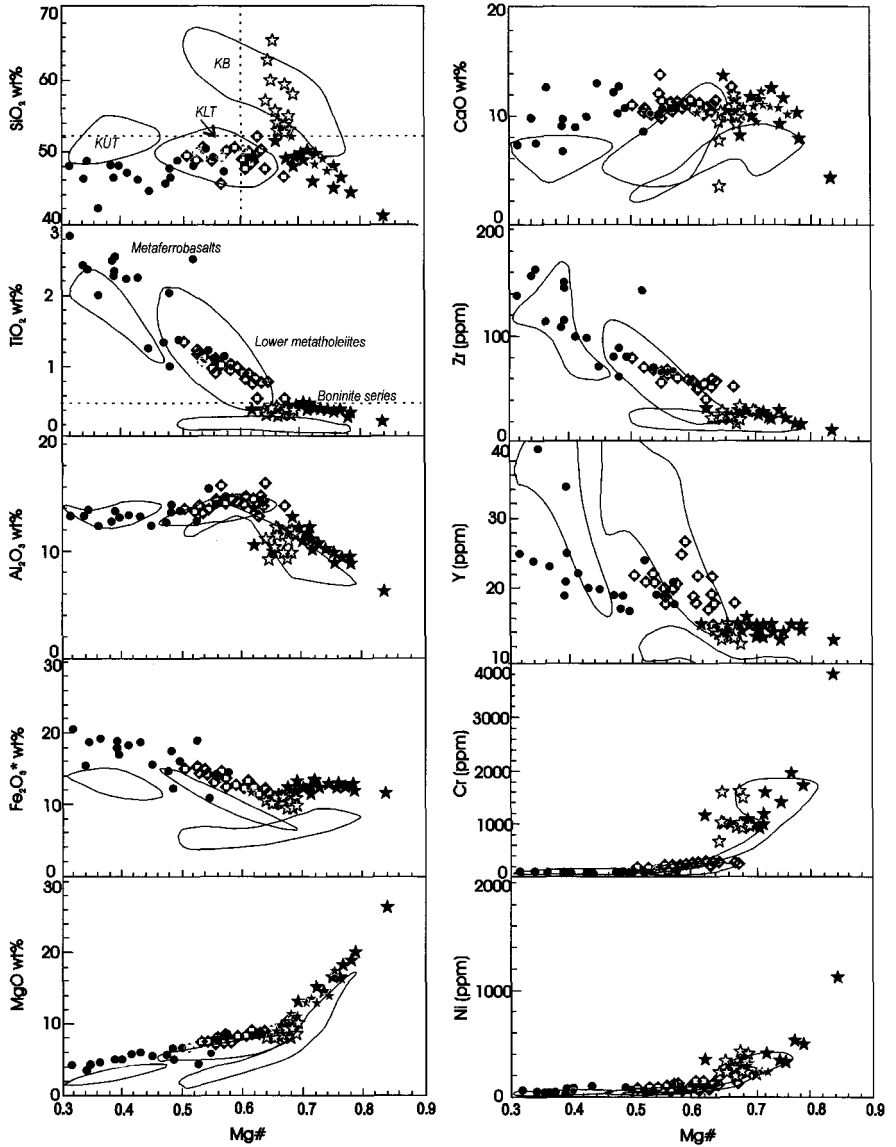


Fig. 15. Mg# variation diagrams for selected major and trace elements showing the three mafic volcanic units from the Khizovaara Northern lithotectonic assemblage. Symbols are as follows: rhombuses, lower tholeiites; white stars and black stars, boninites and associated low-Ti high-Mg basalts, respectively; black circles, Fe-Ti tholeiites. Fields of the Koh SSZ ophiolite (after Meffre et al., 1996) are shown for reference. Abbreviations: KLT = Koh lower tholeiites; KB = Koh boninites; KUT = Koh upper tholeiites. Mg# is calculated as the molecular ratio of $Mg/Mg + Fe^{2+}$. Thin dotted lines show the limit boundaries for the IUGS definition of boninites (Le Bas, 2000).

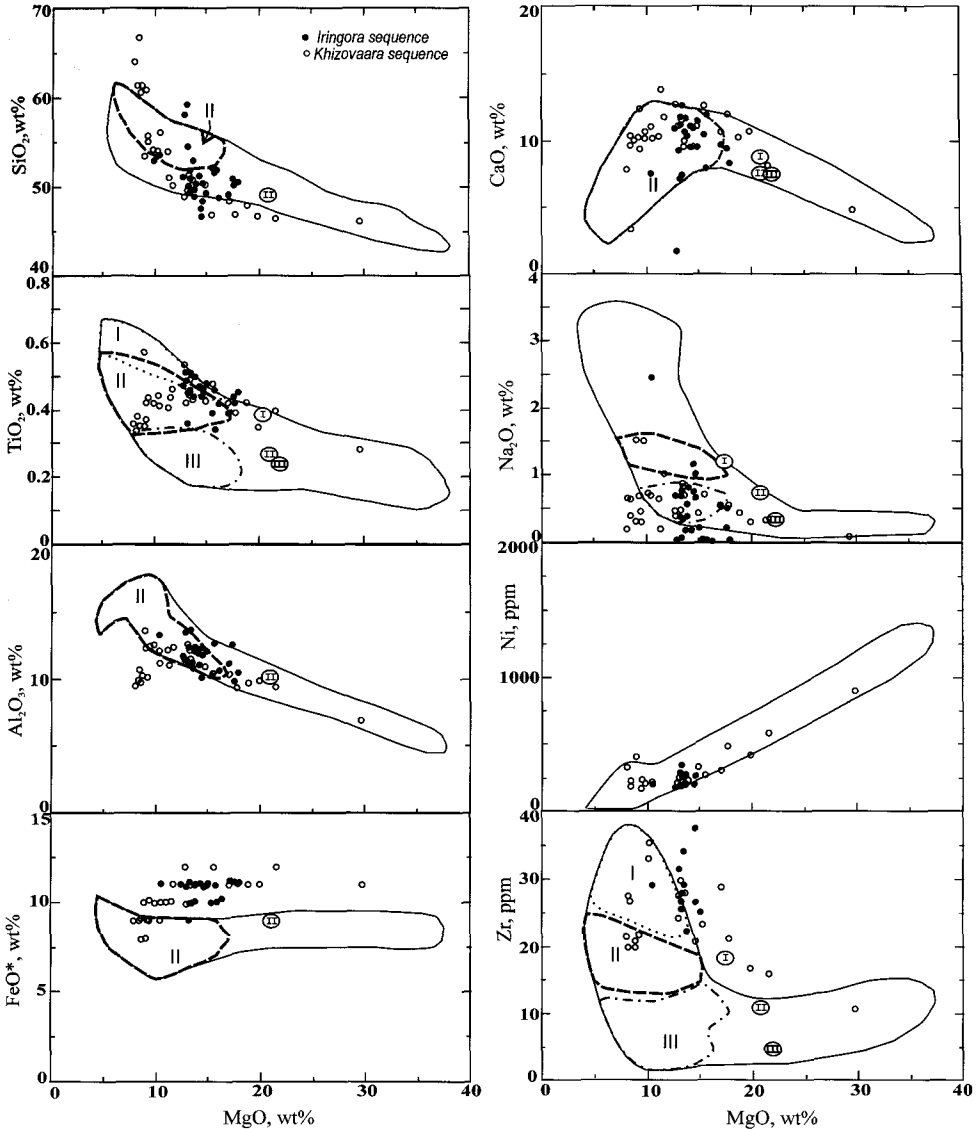


Fig. 16. Major and trace element variation in the NKGB boninite series with MgO (on a volatile-free basis) compared with the composition of Troodos upper pillow lavas (field outlined by solid curve). Fields of three geochemical groups (I–III, respectively) of Troodos UPL are also shown by dotted curves. Fields of Troodos UPL are taken from data compiled by Sobolev et al. (1993) and Cameron (1985). The encircled roman numerals are predicted compositions for the distinct geochemical groups of Troodos parental magmas after Sobolev et al. (1993).

(Meffre et al., 1996) are also shown for reference. It is notable that both the stratigraphic superposition and the geochemical features of the mafic volcanic rocks in the Khizovaara Northern lithotectonic assemblage are principally similar to those of the Koh ophiolite.

This study focused on the NKGB boninite series volcanics because it forms the partially preserved ophiolitic succession of the Iringora Structure. On the other hand, rocks of boninitic affinity are extremely rare in the Early Precambrian. Major and trace geochemistry of the Khizovaara and Iringora boninite series is presented in Tables 3 and 4, respectively. Rocks of boninite series from these two localities are almost geochemically identical. Two continuous rock groups, boninitic and low-Ti tholeiite, can be distinguished based on selected element abundances. The volumetrically dominant low-Ti tholeiites fit in a chemically primitive ($Mg\# = 0.72-0.78$) group of mantle melts strongly depleted in incompatible elements. The group identified as strictly boninitic, including high-Mg hypersthene-normative dacites, is characterized by volatile-free recalculated $SiO_2 = 53.4-66.2$ wt%, $MgO = 8.4-13.1$ wt%, $Mg\# = 0.65-0.74$, and $TiO_2 = 0.34-0.48$ wt%. The relatively high CaO (up to 12.3 wt%) contents and the high CaO/Al_2O_3 values (mostly 0.8-1.1) suggest that they may belong to a high-Ca boninite series (Crawford et al., 1989). The major and trace element geochemical variation of the NKGB boninite series is presented in Fig. 16 where they are compared with the well-known late Cretaceous Upper Pillow Lavas (UPL) of the Troodos ophiolite, Cyprus. It is striking that the compositional range of the 2.8 Ga boninite series volcanics matches the compositional fields of the much younger primitive boninite series lavas. Moreover, in terms of trace element abundance the NKGB boninite series rocks are practically indistinguishable from the geochemical groups I and II (Cameron, 1985) or the groups A and B (Flower and Levine, 1987) of the Troodos UPL (Fig. 17). The sole marked exception is the higher FeO^* contents in the NKGB boninite and related volcanic series as compared with the younger counterparts (Figs. 15, 16). Thus we can infer that a fractional history of parental magma to form the whole stem of the NKGB boninite series was very similar to those postulated for the groups I and II which constitute the major portion of the Troodos ophiolite (Cameron, 1985).

Indeed, the NKGB boninite series volcanics display high abundances of Cr, Ni and Co which vary from 51 to 79 ppm Co, 187-452 ppm Ni, 324-1680 ppm Cr. The early rapid depletion of Cr indicates that chromite was an important early fractionating mineral (Fig. 15). A rapid decrease in Ni with advancing fractionation and increasing of SiO_2 suggests initial crystallization of olivine down to $Mg\# \sim 0.70$ (Fig. 16). As has been emphasized above, these were followed by crystallization of pyroxenes followed, in turn, by plagioclase at $Mg\# < 0.70$. Note that the crystallization of clinopyroxene before plagioclase in these rocks is likely only in a magma with high SiO_2/Al_2O_3 and low CaO/Al_2O_3 ratios, such as rocks of boninitic affinity (Natland, 1981). However, plagioclase appears on the liquidus until a MgO value of $\sim 10\%$ in the NKGB evolving magma, whereas the Troodos counterpart shows a more evolved MgO value of 6% (Cameron, 1985).

True boninite series or contaminated/altered high-Mg rocks? There is a great ambiguity regarding the use of the term "rocks of boninitic affinity" in Archean geology. Crawford et al. (1989) note that very similar major-element compositions exist between modern high-Ca boninites and some previously reported Archean rocks of boninitic affinity, but the

Table 3. Major element oxide (wt%) and trace element abundances (ppm) for the Khizovaara boninite series

Sample	101/1 UM	X-102 BON	X-104 LOTI	X-126/1 BON	X-128 LOTI	X-130 BON	H-302 LOTI	H-305 LOTI	H-319 LOTI	H-320 BON	H-321 BON
SiO ₂	41.25	59.33	45.69	59.84	44.41	55.12	44.31	44.78	49.99	56.68	55.81
TiO ₂	0.25	0.34	0.47	0.37	0.33	0.40	0.38	0.37	0.48	0.34	0.41
Al ₂ O ₃	6.18	9.36	10.11	9.67	9.37	11.02	9.03	8.86	11.78	9.86	11.53
Fe ₂ O ₃ *	11.54	9.21	13.37	10.12	12.10	11.17	12.77	12.31	12.45	9.26	10.68
MnO	0.16	0.16	0.20	0.18	0.19	0.17	0.18	0.19	0.18	0.16	0.17
MgO	26.35	8.31	15.08	8.22	18.92	10.34	20.23	16.67	13.33	8.56	8.98
CaO	4.32	10.04	12.28	9.43	10.23	10.01	7.82	11.36	9.60	9.98	9.98
Na ₂ O	0	0.63	0.70	0.38	0.28	0.70	0.29	0.53	0.84	0.31	0.54
K ₂ O	0.02	0.14	0.08	0.08	0.05	0.09	0.04	0.07	0.07	0.09	0.16
P ₂ O ₅	0.10	0.12	0.14	0.12	0.12	0.13	0.06	0.06	0.07	0.05	0.05
LOI	9.82	2.59	1.95	1.74	3.88	0.93	4.94	4.85	1.21	2.27	1.85
Total	99.99	100.23	100.07	100.15	99.88	100.08	100.05	100.05	100.0	100.06	100.16
Mg#	0.84	0.68	0.72	0.65	0.78	0.68	0.79	0.76	0.71	0.68	0.66
Cr	2840	1680	764	1003	1610	10.67	2150	1780	629	1519	762
Ni	905	452	288	201	423	220	597	495	223	415	306
Co	89.9	72.2	63.2	62.6	73.8	64.0	74.5	74.3	59.6	78.7	77.6
Sc	21	30.8	27.4	43.1	27	45.8	29	28.7	35.8	41.1	36.3
V	142	130	101	265	50	265	213	217	185	251	104
Ba	13.1	47.4	19.3	28.9	7.61	24.5	8.3	13.6	27.4	45.3	59.2
Rb	1.82	2.52	0.67	2.23	0.98	1.43	0.28	0.53	0.53	2.15	2.25
Sr	76.1	102	37.5	61.3	14.3	45.3	26.4	29	98.4	104	82.5

(continued on next page)

Table 3. (Continued)

Sample	101/1 UM	X-102 BON	X-104 LOTI	X-126/1 BON	X-128 LOTI	X-130 BON	H-302 LOTI	H-305 LOTI	H-319 LOTI	H-320 BON	H-321 BON
Nb	0.251	0.670	0.696	1.040	0.620	0.910	0.639	0.662	0.742	0.787	0.754
Hf	0.250	0.71	0.73	0.74	0.43	0.81	0.46	0.68	0.76	0.67	0.62
Zr	10.8	20.70	23.31	27.70	16.81	32.97	16.27	21.35	27.78	20.96	19.98
Y	3.74	9.73	9.60	12.90	8.40	14.1	8.58	9.12	11.30	12.40	11.00
Th	0.052	0.081	0.115	0.174	0.075	0.155	0.098	0.074	0.186	0.098	0.082
U	0.009	0.032	0.027	0.040	0.022	0.028	0.026	0.016	0.035	0.030	0.038
La	0.349	1.030	1.110	1.120	0.776	1.150	0.948	1.010	1.370	1.330	1.040
Ce	0.882	2.640	3.100	2.650	2.190	3.330	2.460	2.590	3.500	3.390	2.840
Pr	0.131	0.441	0.460	0.465	0.377	0.575	0.400	0.388	0.506	0.578	0.425
Nd	0.832	2.440	2.452	2.790	2.050	2.850	2.240	2.140	2.730	2.620	2.380
Sm	0.341	0.935	0.909	1.140	0.826	1.060	0.799	0.811	0.991	1.070	0.900
Eu	0.086	0.447	0.362	0.401	0.355	0.323	0.316	0.320	0.384	0.468	0.402
Gd	0.429	1.200	1.280	1.350	1.040	1.520	1.150	1.130	1.380	1.310	1.270
Tb	0.109	0.248	0.249	0.274	0.236	0.274	0.235	0.233	0.329	0.261	0.271
Dy	0.693	1.740	1.820	2.160	1.490	2.200	1.560	1.510	2.010	1.910	1.830
Ho	0.161	0.390	0.403	0.434	0.350	0.513	0.362	0.367	0.445	0.404	0.433
Er	0.421	1.210	1.110	1.150	1.130	1.370	1.040	1.140	1.370	1.420	1.200
Tm	0.089	1.840	0.119	0.214	0.152	0.228	0.167	0.149	0.199	0.207	0.194
Yb	0.449	1.090	1.170	1.370	1.140	1.440	1.010	0.939	1.190	1.270	1.220
Lu	0.525	0.387	0.187	0.199	0.170	0.200	0.144	0.153	0.412	0.168	0.174
La/YbN	0.525	0.638	0.640	0.552	0.459	0.539	0.634	0.726	0.777	0.707	0.575
La/SmN	0.644	0.694	0.679	0.619	0.591	0.683	0.747	0.784	0.870	0.783	0.728
Gd/YbN	0.772	0.890	0.884	0.796	0.737	0.853	0.920	0.971	0.937	0.834	0.841

(continued on next page)

Table 3. (Continued)

Sample	H-323 BON	H-324 LOTI	H-325 LOTI	H-325/1 BON	H-326 BON	H-332 FEL	H-334/1 BON	H-334/2 LOTI	H-334 LOTI	H-333 LOTI	H-335 FEL
SiO ₂	53.66	49.37	48.78	54.10	53.00	65.69	59.36	49.64	49.91	47.13	62.66
TiO ₂	0.40	0.42	0.42	0.42	0.43	0.33	0.36	0.42	0.43	0.41	0.35
Al ₂ O ₃	11.86	10.6	12.31	12.19	11.92	10.45	9.92	11.88	11.21	10.08	9.32
Fe ₂ O ₃ *	9.87	12.27	11.87	11.10	10.76	10.15	9.89	12.57	11.62	12.93	9.98
MnO	0.18	0.19	0.20	0.17	0.17	0.16	0.16	0.18	0.18	0.18	0.15
MgO	8.95	14.57	12.66	9.21	10.13	8.31	9.04	13.32	12.92	16.59	7.95
CaO	11.91	10.88	10.91	10.02	10.89	3.34	9.19	9.85	11.39	10.48	7.67
Na ₂ O	0.29	0.41	0.46	0.42	0.69	0.61	0.65	0.68	0.44	0.49	0.18
K ₂ O	0.06	0.09	0.49	0.42	0.17	0.13	0.07	0.08	0.09	0.06	0.16
P ₂ O ₅	0.07	0.05	0.07	0.05	0.07	0.04	0.07	0.07	0.07	0.05	0.06
LOI	2.76	1.16	1.84	2.02	1.83	0.79	1.43	1.33	1.75	1.62	1.73
Total	100.01	100.01	100.01	100.12	100.0	100.0	100.14	100.02	100.0	100.02	100.21
Mg#	0.68	0.72	0.71	0.66	0.69	0.66	0.68	0.71	0.72	0.75	0.65
Cr	688	1040	939	996	912	977	919	960	1199	1412	1603
Ni	221	346	223	215	219	226	191	217	241	325	342
Co	63.7	69.6	63.4	67.5	66.8	66.7	62.3	64.5	64.2	72.2	77.9
Sc	34.2	34.3	42.9	52.3	47.9	48.0	46.4	44.9	43.8	40.8	45.7
V	126	201	244	277	254	228	223	214	233	167	179
Ba	36.4	28.1	103	342	23.8	45.1	31.5	15.5	17.2	8.77	37.6
Rb	1.26	1.47	24.7	42.4	2.66	7.38	0.74	0.39	0.42	1.01	6.84
Sr	54.7	27	73.2	85.3	127	37.2	73.5	43.5	76.7	25.5	55.2

(continued on next page)

Table 3. (Continued)

Sample	101/1 UM	X-102 BON	X-104 LOTI	X-126/1 BON	X-128 LOTI	X-130 BON	H-302 LOTI	H-305 LOTI	H-319 LOTI	H-320 BON	H-321 BON
Nb	0.810	0.595	0.948	0.986	0.971	1.100	0.865	0.877	0.876	0.821	0.818
Hf	0.46	0.66	0.69	0.59	0.89	0.74	0.75	0.66	0.76	0.70	0.68
Zr	15.8	20.63	24.03	21.33	35.21	27.78	26.53	18.26	27.78	25.26	21.23
Y	10.7	9.82	13.70	13.10	14.8	11.0	14.5	13.3	13.0	12.8	13.6
Th	0.099	0.084	0.097	0.153	0.122	0.137	0.065	0.114	0.083	0.121	0.113
U	0.025	0.020	0.021	0.045	0.041	0.019	0.008	0.031	0.029	0.027	0.026
La	1.080	0.931	1.250	1.160	1.400	1.990	1.340	1.310	1.610	1.170	1.440
Ce	2.790	2.560	3.210	2.940	3.580	4.820	3.590	3.450	3.620	3.020	3.510
Pr	0.448	0.400	0.524	0.460	0.599	0.712	0.540	0.574	0.606	0.496	0.587
Nd	2.430	2.180	2.840	2.450	2.960	3.260	2.950	2.910	2.890	2.580	2.400
Sm	0.902	0.804	0.988	0.941	1.070	1.120	1.060	1.030	0.959	0.983	0.987
Eu	0.339	0.345	0.407	0.388	0.450	0.182	0.372	0.315	0.448	0.373	0.261
Gd	1.270	1.180	1.500	1.310	1.510	1.460	1.540	1.430	1.540	1.220	1.420
Tb	0.259	0.254	0.283	0.242	0.298	0.267	0.271	0.268	0.277	0.225	0.274
Dy	1.860	1.620	2.100	1.900	2.060	1.800	2.200	1.990	2.130	1.870	1.900
Ho	0.416	0.343	0.453	0.450	0.473	0.491	0.500	0.451	0.455	0.387	0.469
Er	1.300	1.040	1.390	1.250	1.560	1.450	1.420	1.470	1.340	1.300	1.390
Tm	0.231	0.174	0.204	0.211	0.244	0.228	0.216	0.194	0.213	0.206	0.229
Yb	1.300	1.170	1.350	1.360	1.680	1.340	1.480	1.380	1.370	1.020	1.130
Lu	0.173	0.157	0.203	0.280	0.206	0.221	0.259	0.211	0.201	0.176	0.177
La/YbN	0.561	0.537	0.625	0.576	0.563	1.002	0.611	0.641	0.793	0.774	0.860
La/SmN	0.754	0.723	0.797	0.776	0.824	1.119	0.796	0.800	1.057	0.672	0.919
Gd/YbN	0.789	0.937	0.898	0.778	0.726	0.880	0.841	0.873	0.908	0.967	1.016

Abbreviations: UM, ultramafic (cumulate?) rock; LOTI, low-Ti tholeiite; BON, boninite; FEL, felsic rocks of boninite series; LOI, loss on ignition.

Table 4. Major element oxide (wt%) and trace element abundances (ppm) for the Iringora SSZ ophiolite sequence

Sample	Lava unit					Dike unit			Gabbro unit	
	I-417	I-417/2	I-427	I-427/1	I-429	I-415	I-418/1	I-419/1	I-419	I-429/1
SiO ₂	49.16	47.54	52.80	49.15	52.83	47.59	49.95	57.52	50.31	50.83
TiO ₂	0.42	0.44	0.47	0.47	0.44	0.46	0.33	0.35	0.50	0.42
Al ₂ O ₃	10.65	10.00	13.03	11.41	10.73	11.63	8.64	9.39	13.53	10.35
Fe ₂ O ₃ *	12.25	12.77	12.13	12.76	11.60	12.46	11.15	10.51	12.56	11.53
MnO	0.19	0.19	0.17	0.18	0.15	0.18	0.18	0.17	0.18	0.17
MgO	12.92	14.54	10.35	14.20	12.75	13.68	15.24	12.80	13.00	13.14
CaO	11.37	10.84	7.33	9.14	8.88	11.02	11.45	6.86	7.09	10.09
Na ₂ O	0.35	0.77	2.44	1.00	0.38	0.24	0.01	0.07	0.86	0.19
K ₂ O	0.07	0.05	0.08	0.06	0.11	0.15	0.09	0.10	0.12	0.17
P ₂ O ₅	0.13	0.09	0.10	0.12	0.12	0.09	0.09	0.08	0.10	0.10
LOI	2.52	2.85	1.11	1.54	2.10	2.56	2.96	2.21	1.82	3.05
Total	100.03	100.08	100.01	100.03	100.09	100.06	100.09	100.06	100.07	100.04
Mg#	0.71	0.73	0.66	0.72	0.72	0.72	0.76	0.74	0.71	0.72
Cr	705.56	543.17	323.79	672.52	789.42	644.72	972.42	538.78	612.72	708.17
Ni	254.40	191.59	186.67	256.84	280.60	215.40	326.12	188.67	164.33	265.90
Co	74.10	72.03	52.56	71.57	70.79	66.37	60.72	50.72	57.85	66.10
Sc	37.83	36.32	39.93	38.56	36.26	40.69	29.11	32.63	44.58	33.23
V	237.95	233.21	338.38	297.40	311.42	251.49	186.10	202.43	296.20	267.17
Ba	15.76	26.11	17.68	15.24	34.21	56.94	26.84	11.56	20.48	42.03
Rb	0.92	1.03	1.19	0.82	1.93	7.82	2.31	2.63	2.76	5.78
Sr	49.30	31.27	62.49	61.22	74.04	101.85	107.84	69.50	170.78	92.96
Nb	0.88	0.78	1.01	0.96	0.71	1.01	0.73	1.06	1.08	0.88
Hf	0.89	0.72	0.83	1.04	0.71	0.66	0.72	0.75	0.85	0.73
Zr	33.92	26.42	28.96	37.91	25.47	24.96	26.67	26.54	28.89	22.06
Y	12.20	12.37	13.87	12.94	10.05	13.94	10.07	12.23	15.41	11.71
Th	0.09	0.07	0.13	0.11	0.11	0.15	0.13	0.17	0.13	0.12
U	0.04	0.03	0.04	0.04	0.03	0.04	0.06	0.08	0.03	0.03
La	0.78	1.04	1.16	1.03	1.11	1.37	1.16	1.39	1.34	1.12
Ce	2.51	2.96	3.49	3.13	2.87	3.68	3.13	3.55	3.76	3.23
Pr	0.39	0.45	0.55	0.53	0.41	0.53	0.41	0.52	0.56	0.54
Nd	2.05	2.55	3.42	2.68	2.12	2.77	2.25	2.57	3.33	2.73
Sm	0.73	0.79	0.99	0.87	0.68	0.84	0.72	0.82	1.01	0.93
Eu	0.35	0.40	0.39	0.32	0.46	0.43	0.36	0.29	0.40	0.34
Gd	1.31	1.34	1.62	1.46	1.18	1.38	1.19	1.37	1.60	1.41
Tb	0.24	0.23	0.27	0.23	0.22	0.25	0.20	0.27	0.32	0.25
Dy	1.77	1.74	2.03	1.90	1.44	1.84	1.51	1.78	2.36	1.75
Ho	0.41	0.39	0.45	0.41	0.35	0.46	0.33	0.43	0.51	0.42
Er	1.20	1.19	1.32	1.22	1.02	1.22	0.93	1.26	1.42	1.17
Tm	0.17	0.17	0.18	0.16	0.15	0.20	0.12	0.19	0.21	0.19
Yb	1.05	1.08	1.24	1.18	0.96	1.28	0.81	1.18	1.48	1.25
Lu	0.15	0.14	0.19	0.17	0.14	0.17	0.13	0.19	0.21	0.17
La/Yb _N	0.501	0.650	0.631	0.589	0.781	0.722	0.967	0.795	0.611	0.605
La/Sm _N	0.829	0.829	0.738	0.745	1.028	1.027	1.014	1.067	0.835	0.758
Gd/Yb _N	1.008	1.003	1.056	1.000	0.993	0.871	1.187	0.938	0.874	0.916

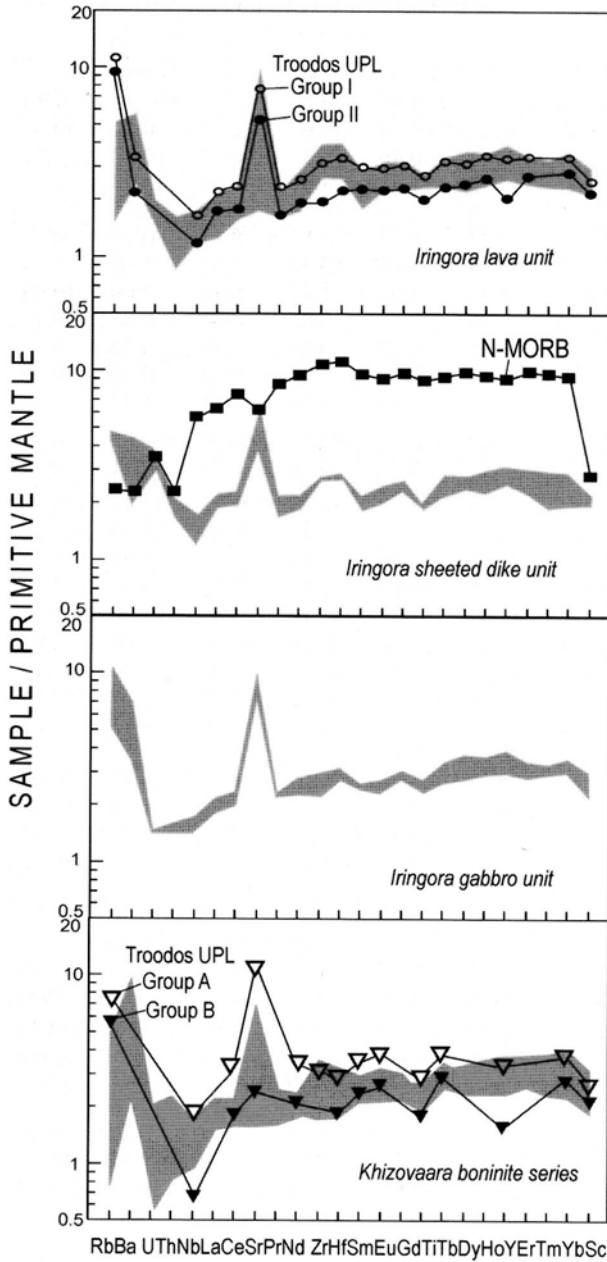


Fig. 17. Geochemical compositions of the Iringora and Khizovaara boninite series compared Troodos UP lavas. Primitive mantle and N-MORB abundances are taken from Hofmann (1988).

latter have obviously formed by other ways. Indeed, high-Mg rocks with unusually high SiO_2 of up to 58% have been described in the 3.4 Ga Nondweni greenstone belt, South Africa as komatiitic andesites (Riganti and Wilson, 1995) and in some late Archean and early Proterozoic greenstone belts as siliceous high-Mg basalts (SHMB) (Sun et al., 1989). However these are commonly believed to form when ultramafic (komatiitic) magmas have undergone crustal contamination and subsequent fractional crystallization (e.g., Arndt et al., 1997; Sylvester et al., 1997). This leads to the question of whether the NKGB suite of high-Ca boninitic affinity belongs to a true boninite series or it represents an unusual kind of crustally contaminated high-Mg rock of komatiitic affinity.

There are several lines of evidence to show that the NKGB suite is not crustally contaminated komatiite-derived magma. Ratios of Ti to the adjacent transition elements Sc and V in the former are lower than in MORB, komatiites or komatiitic basalts and SHMB and close to the primitive mantle ratios (Fig. 18a). Although Zr/Ti ratios vary between 70 and 140 and tend to be also centered around the primitive mantle ratio (~ 110), the NKGB suite fields on a plot of Zr vs. TiO_2 are far lower than a typical N-MORB and markedly distinct from the field of SHMB (Fig. 18b). Contrary to overall LREE-enriched SHMB, the NKGB boninite series volcanics are relatively depleted in LREE compared to the primitive mantle abundances and range in $(\text{La}/\text{Yb})_{\text{N}}$ from 0.5 to 1.0 mostly being between 0.6 and 0.8, whereas HREEs show less depleted patterns ($\text{Ga}/\text{Yb}_{\text{N}} = 0.8\text{--}1$). There are also variable negative Nb anomalies (av. $\text{Nb}^*/\text{Nb} = 0.59$) but dominantly positive Zr and Hf peaks (av. $\text{Zr}^*/\text{Zr} = 1.14$ and av. $\text{Hf}^*/\text{Hf} = 1.13$), additional distinctive features of many recent boninite series (Hickey and Frey, 1982; Pearce et al., 1999). Mantle-normalized plots (Figs. 19a, b) summarize many of distinctive features shared between the NKGB boninitic rocks and younger high-Ca boninites. Conversely, they display crucial differences as compared with crustally contaminated komatiite-derived counterparts (Fig. 19c).

Finally, Sm-Nd isotope investigations were carried out to verify constraints on the source composition that formed the NKGB boninite series volcanics. As can be seen from Table 5, all the analyzed samples from the Khizovaara Structure bear positive ϵ_{Nd} values strongly suggesting that no older felsic crust was involved in their petrogenesis and implying, therefore, that they developed in an intraoceanic setting. In contrast, crustally contaminated komatiite-derived lavas yield almost negative ϵ_{Nd} values (e.g., Sun et al., 1989; Riganti and Wilson, 1995; Arndt et al., 1997; Puchtel et al., 1997). However the range of ϵ_{Nd} values is wide in the Khizovaara boninite series rocks (from +3.28 to +1.10). A majority of the boninitic samples have initial $^{143}\text{Nd}/^{144}\text{Nd}$ ratios of between 1.36 and 1.10 whereas the most primitive composition of sample X-128 yields ϵ_{Nd} value of 3.28. Taking into account the mean ϵ_{Nd} value of about 3.0 ± 0.5 for a Neoproterozoic long-term depleted mantle reservoir (e.g., Puchtel et al., 1997, and references therein), it is apparent that the Khizovaara boninites are twice as enriched in a low-radiogenic Nd component. Surprisingly, the same rate of the enrichment relative to the MORB source is typical of the group II Troodos UPL that is believed to have resulted from an addition of small amounts (up to 5%) of LREE-enriched subduction component (Cameron, 1985). Despite few data, the inverse correlation between ϵ_{Nd} and a rate of Hf enrichment relative to REE represented by

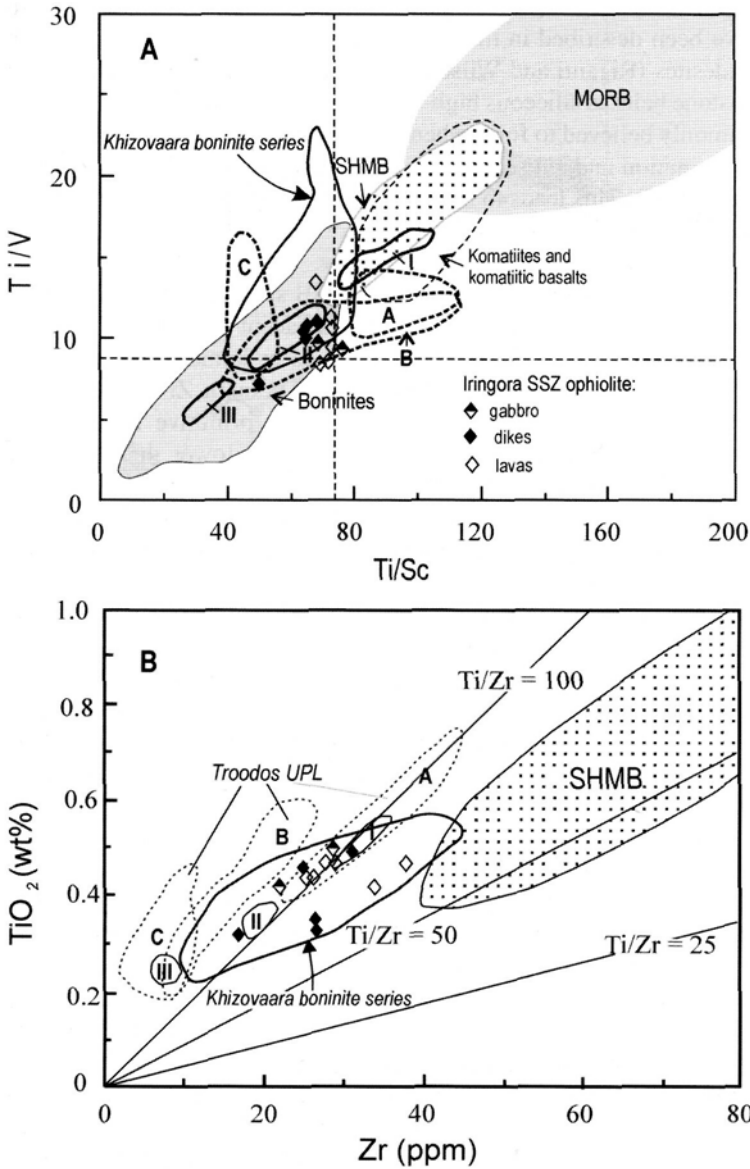


Fig. 18. Ti/V vs. Ti/Sc (A) and TiO₂ vs. Zr (B) plots for the Khizovaara (shown by the fields) and the Iringora (shown by rhombus) boninite series. For comparison fields of Troodos UPL also are shown: groups I, II and III from Cameron (1985); groups A, B and C from Flower and Levine (1987). Fields for boninites, komatiites, MORB and SHMB are from the compilation of Poidevin (1994). Dashed lines indicate primitive mantle ratios.

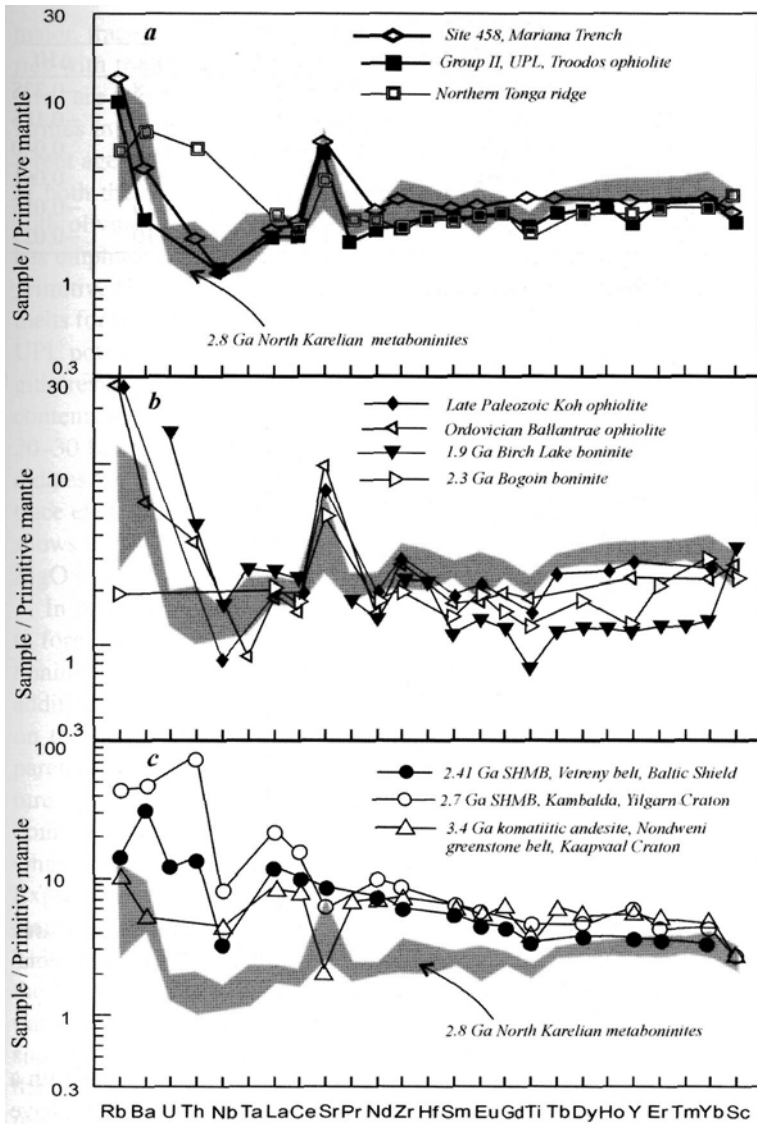


Fig. 19. Comparison of mantle-normalized trace-element abundance patterns of North Karelian boninites with recent (a), Phanerozoic and Paleoproterozoic (b) high-Ca boninites and Paleoproterozoic and Archean komatiite-derived crustally contaminated counterparts (c). Data sources are as follows: Mariana Trench (Hickey and Frey, 1982); Troodos ophiolite (Cameron, 1985); Northern Tonga ridge (Sobolev and Danyushevsky, 1994); Koh ophiolite (Meffre et al., 1996); Ballantrae ophiolite (Smellie et al., 1995); Birch Lake boninite (Wyman, 1999); Bogoin boninite (Poidevin, 1994); Vetreny belt (Puchtel et al., 1997); Kambalda (Jochum et al., 1990); Nondweni belt (Riganti and Wilson, 1995).

Table 5. Sm-Nd isotopic data for the 2.8 Ga Khizovaara boninite series volcanics

Sample	Sm, ppm	Nd, ppm	$^{147}\text{Sm}/^{144}\text{Nd}$	$^{143}\text{Nd}/^{144}\text{Nd}$	ϵ_{Nd}	ΔHf
X-128	0.96	2.59	0.22301	0.513291	3.28	-0.338
H-325/1	0.72	1.92	0.22651	0.513315	2.48	-0.185
X-130	0.71	1.82	0.23718	0.513455	1.36	0.040
H-326	0.87	2.27	0.23265	0.513370	1.33	0.061
H-320	0.79	2.04	0.23507	0.513411	1.26	-0.055
X-126/1	0.68	1.72	0.23857	0.513468	1.10	-0.021

Note: ΔHf was calculated from Hf, Nd and Yb abundances listed in Table 3.

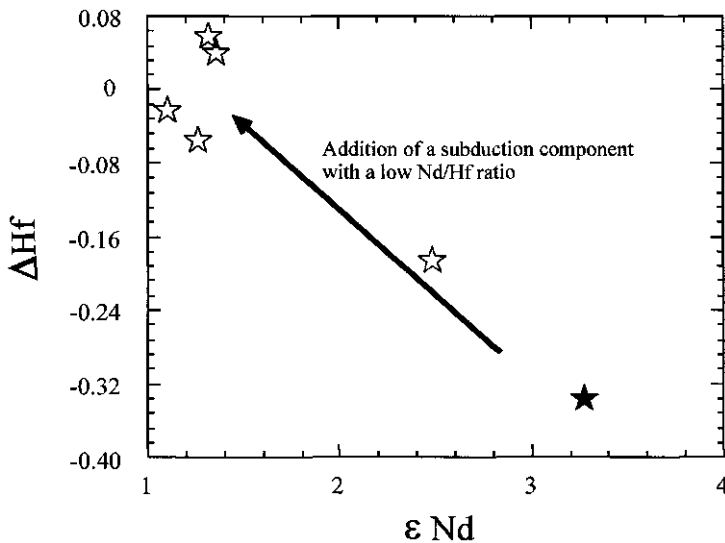


Fig. 20. $\epsilon_{\text{Nd}}-\Delta\text{Hf}$ covariations in the Khizovaara boninite series rocks. ΔHf expression is after Pearce et al. (1999). Symbols are as follows: white stars, evolved ($\text{Mg}\# = 0.65-0.69$) boninitic compositions; black star, primitive ($\text{Mg}\# = 0.78$) high-Mg low-Ti tholeiitic composition.

Hf (Pearce et al., 1999) occurs (Fig. 20). This implies that a subduction component with a low Nd/Hf ratio was involved in the NKGB boninite series melts. Pearce et al. (1999) have explained the nature of such enrichment by two-stage mantle melting processes. A first stage of melting depletes the mantle source through extraction of melts with a high Nd/Hf ratio. The second stage of melting that produces boninites would then give melts with low Nd/Hf ratio.

Origin of the NKGB boninite series. There is a general consensus that the origin of boninites requires a water-saturated high-temperature melting of a mantle wedge that has been depleted by incompatible elements by previous melting episodes (Crawford et al., 1989, and reference therein). Data expressed above strongly suggest that a similarity in

major, trace element and isotope chemistry exist when compared the NKGB boninite series with the Cretaceous Troodos ophiolitic lavas. It is vital to note that the Troodos UP lavas are taken as type high-Ca boninite suite (Crawford et al., 1989). The amazing similarities in major- and trace element chemistry along the boninite series of drastically different ages reflect their similar petrogenetic processes. Comparison of fractional histories of both these series strongly suggests that compositionally similar melts in equilibrium with olivine were parental melts for the entire high-Ca boninite series. Cameron (1985) has emphasized that the stem of Troodos UPL boninite series was evolved from the most primitive low-SiO₂ end-member. Nevertheless there is no agreement regarding the parental melts for the boninite series. Duncan and Green (1980a, 1980b) have shown that a Troodos UPL potential parental magma with 15–16% MgO could have segregated from a harzburgitic residue at 7–8 kbar and 1360 °C. Other estimates suggest that this might have MgO contents in the range 17–22%, generated in a mantle wedge above a subduction zone at 20–30 kbar and 1380–1550 °C (Sobolev et al., 1993). Comparison of the potential candidates for NKGB boninite series primary melts with the available data on the predicted trace element characteristics for Troodos UPL parental magmas (cf. Sobolev et al., 1993) shows a close approximation to the latter constraint. This enables us to suggest that the MgO contents for the NKGB boninite series primary melts of about 20% are permissible.

In order to constraint the P-T conditions under which parental melts were generated to form the NKGB boninite series, its composition coupled together with fields of recent boninite series are plotted on Walker's ternary projection (Walker et al., 1979) (Fig. 21). In addition, available experimental data on the dry and wet mantle melting are also shown on the diagram. As can be seen from the diagram, under dry conditions the predicted parental melts should be formed at pressures of about 3 Gpa and a potential temperature close to 1550 °C. However it is common knowledge that initial water contents in boninitic parental magmas might lay in a range of 1–3% (e.g., Crawford et al., 1989; Ohnenstetter and Brown, 1996) that must depress to some extent the peridotite solidus. Experimental data of Kushiro (1990) suggest a 0.2 Gpa depression of the solidus for a mantle with 4.4–6.6% H₂O that corresponds to a temperature lowering of nearly 150 °C. This implies that a starting melting of a previously depleted mantle wedge to have formed the NKGB boninite series could be realized at a pressure of nearly 2.0 Gpa and a potential temperature less than 1450 °C. Furthermore the NKGB boninite series parental melts should be having some water excess as compared with the younger counterparts. Indeed, the overall NKGB boninite series trend tends to in progress towards the Qz apex (Fig. 21) implying, therefore, that it could be developed with more H₂O content respectively to the recent ones. This may also indicate that the more evolved portions of the NKGB boninite series were crystallized in the amphibole-in stability field.

In summary, all the data expressed above strongly suggest that there is no substantial difference between the generation conditions of the Neoproterozoic and recent high-Ca boninite series counterparts. The only difference between them is a lack of analogues to the most depleted group III of Troodos UPL in the NKGB counterpart. However, among other reasons, this may be due to a sampling gap of the latter when compared with a huge amount of sampling which has been done in the Troodos ophiolite.

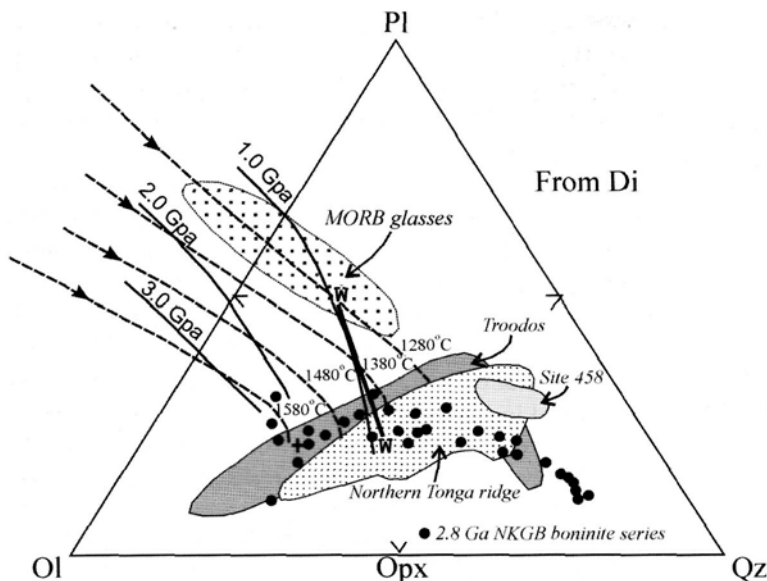


Fig. 21. Normative compositions of the North Karelian boninite series in ternary projection olivine-plagioclase-quartz from diopside (Walker et al., 1979). Predicted composition for NKGB parental magmas indicated by the cross. The fields for the Phanerozoic high-Ca boninite series and MORB glasses are shown for reference. The data sources used here are as follows: Cameron (1985), Sobolev et al. (1993) for the Troodos Massif; Fallon and Crawford (1991) and Sobolev and Danyushevsky (1994) for the northern Tonga trench; Mickey and Frey (1982) for the site 458 of DSDP, Mariana trench. The field of MORB glass data ($\text{MgO} > 9 \text{ wt}\%$) is taken from Elton (1989). Compositional trends from the experimental and calculated data on upper mantle melting are shown to constraint P-T generation conditions of the NKGB boninite series. The isobaric compositional trends under dry conditions for 1, 2, 3 Gpa are taken from Hirose and Kushiro (1993). Solid line labeled as W-W is the isobaric compositional trend under the wet conditions (for an H_2O content of 4.4-6.6 wt% at 1.2 Gpa) from Kushiro (1990). Dotted lines are point average compositions for various upper mantle potential temperatures (1580-1280 °C) from McKenzie and Bickle (1988).

3.2. Geochemistry of the Arc-Related Volcanics

Most geochemical data on the NKGB acid-felsic volcanics comes from the Khizovaara Structure. Two distinct volcanic rock suites are recognized based both on field appearance and compositional characteristics. These are called the Northern andesite suite and the Southern andesite-dacite-rhyolite suite (Figs. 2, 3). In addition, two distinct plutonic suites, the Northern and the Southern tonalites, surround the Khizovaara greenstones.

The Northern andesite suite consists mostly of massive, amygdaloidal, glomeroporphyritic textured andesites. In terms of major element chemistry the Northern andesites are characterized by low Al_2O_3 and high Na_2O contents and belong to the tholeiitic magma clan (Thurston and Kozhevnikov, 2000). However, based upon the trace element grounds

they define three separate groups being as follows: 'depleted andesite', 'enriched andesite' and 'high-Nb andesite' (Figs. 22, 24). The 'depleted andesite' (NAD) group volumetrically prevails. This yields high MgO, Cr and Ni contents and conversely low abundances of LILE, HFSE and REE (Table 6). The trace element patterns show flat to slightly fractionated REE ($\text{La/Sm}_N = 0.79\text{--}1.9$, $\text{Gd/Yb}_N = 1.5\text{--}1.9$) coupled with negative anomalies of Eu, Nb and Ti (Fig. 24). The 'enriched andesite' group (NAE) is found along both flanks of the unit. As compared with the above this is depleted in MgO and Cr and conversely enriched in LILE, HFSE and LREE ($\text{La/Sm}_N = 3.3\text{--}4.1$, $\text{Gd/Yb}_N = 1.7\text{--}2.1$) and characterized also by the pronounced negative Nb anomalies. The 'high-Nb andesite' (NANb) group occurs only along with the south contact of the unit with the Southern lithotectonic assemblage. Compositionally this group is similar to the enriched andesites. With respect to the latter it is characterized by lower MgO contents, higher REE abundances fractionated in a different manner ($\text{La/Sm}_N = 2.8\text{--}3.0$, $\text{Gd/Yb}_N = 1.7\text{--}2.1$), and enrichment in Ti, Zr and Nb (Figs. 22, 24). Note that such enrichment is accompanied by lower ratios of Ti/Nb, Zr/Nb and Ti/Zr as compared with the 'enriched andesite' group (Table 6).

Because the trace elements outlined above are commonly treated as practically immobile during low-temperature alteration and metamorphism, their variations might be due to magmatic processes. Most of the major and trace elements reveal similar covariations throughout the three geochemical groups. This suggests similar fractionation histories of their parental melts. Modeling of possible fractionation paths has shown that a liquidus assemblage of plagioclase + pyroxene \pm olivine \pm amphibole \pm Fe-Ti oxides could control a crystal differentiation of parental melts with low H₂O contents at shallow-level depths (< 30–40 km) to reach the observed major element variations. However the trace element patterns cannot be explained by crystal fractionation alone. Indeed, the low concentrations of SiO₂ coupled together with the high abundances of siderophylic elements (Table 6) suggest an ultramafic precursor rather than a mafic one for their parental melts. Thus the 'depleted andesite' group appears to have formed through a partial melting of previously depleted mantle precursor in a manner similar with that generated boninitic melts. In contrast, the trace element pattern of the 'enriched andesite' group (Fig. 24) gives an indication of a LREE enriched metasomatic component involved in a melting of depleted mantle. The 'high-Nb andesite' group exhibits a remarkable enrichment in both LREE and HFSE, much as the neighbouring Fe-Ti basalts display. It should be noted also their high Gd/Yb_N ratios are suggestive of garnet in the mantle residue and, therefore, imply that this might be because they formed at deeper levels (> 70 km) as compared with the other andesitic counterparts. In addition, trends to high MgO, Cr, Ni coupled together with negative Nb spikes (Figs. 22, 24) can be accounted for by interaction between different siliceous slab melts and a subarc mantle wedge. It is amazing that amongst recent counterparts the geochemistry of the Northern andesite suit is best matched to that of the so-called high-Ti series lavas of the Troodos ophiolite (cf. Staudigel et al., 1999).

The Northern tonalite suite combines a variety of plutonic rocks that border the Khizovaara greenstones on the north (Fig. 2). It ranges from tonalite to trondhjemite (NT) (Fig. 22) and is accompanied by numerous co-genetic tonalitic dikes (NTD) emplaced into the Northern lithotectonic assemblage. These are characterized by high Al₂O₃, Sr and

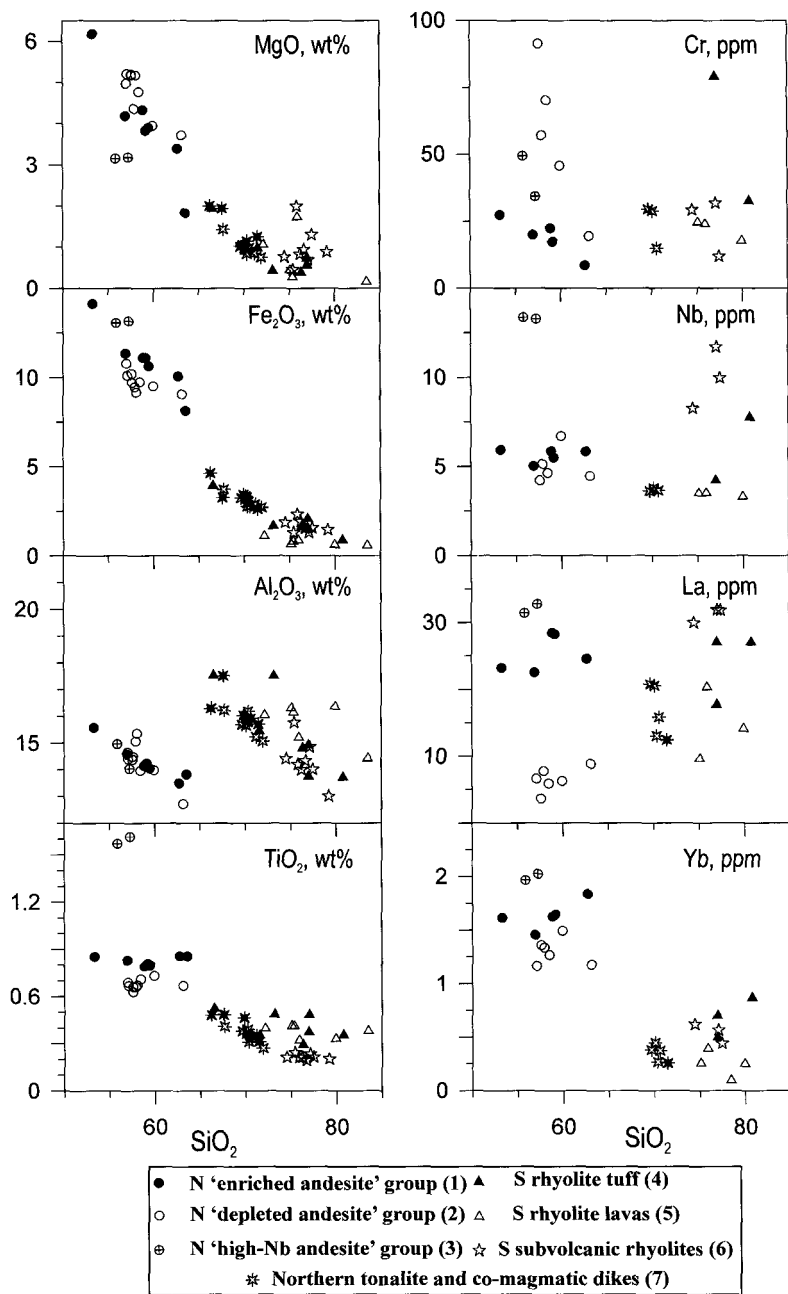


Fig. 22. Harker compositional diagrams showing selected major and trace element variations for Northern andesite and tonalite suites, and Southern rhyolites of the Khizovaara structure.

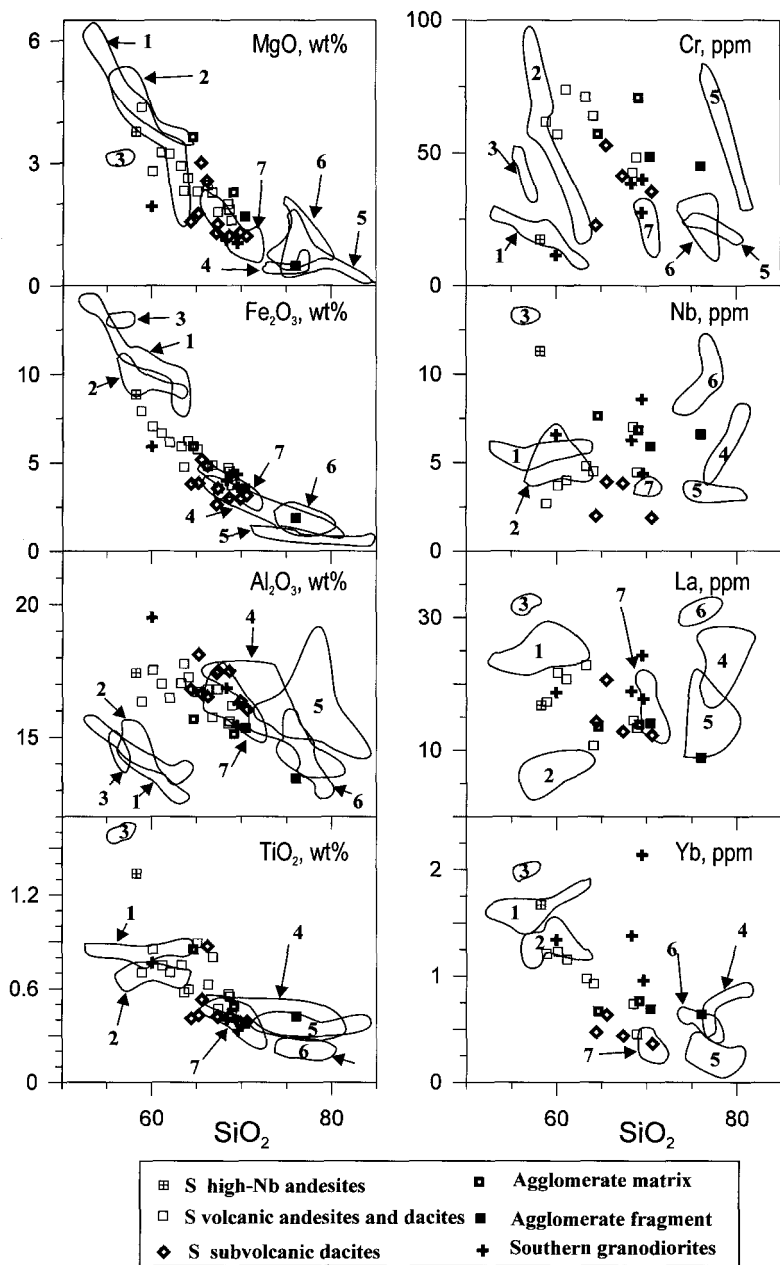


Fig. 23. Harker compositional diagrams showing selected major and trace element variations for the Southern andesite-dacite and granodiorite suite. Fields labeled by numbers correspond to the compositions of Fig. 23 and are shown for reference.

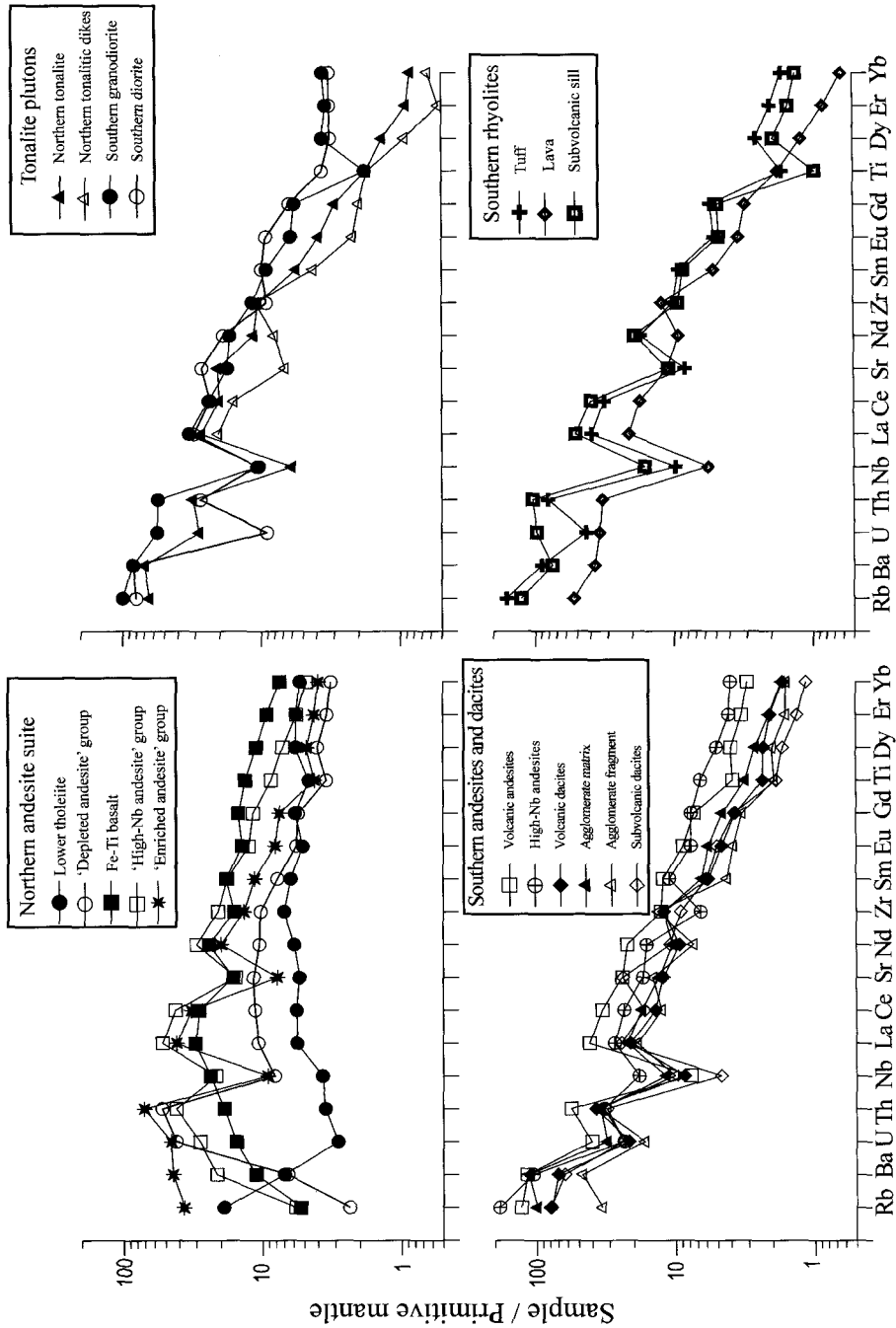


Fig. 24. Trace-element spidergrams for Khizovaara acid-felsic rocks normalized to primitive mantle values of Hofmann (1988).

Table 6. Mean abundances of major element oxides (wt%) and trace elements (ppm) for the Khizovaara arc-derived volcanic and plutonic rocks

Rock type <i>n</i>	NAE 7	NAD 9	NA(Nb) 2	NT 8	NTD 5	SA(Nb) 1	SA 6	SD 8
SiO ₂	59.14	58.54	56.57	70.24	69.11	58.27	61.16	66.98
TiO ₂	0.83	0.68	1.59	0.35	0.42	1.34	0.75	0.62
Al ₂ O ₃	14.29	14.35	14.51	15.73	16.30	17.42	17.00	16.32
Fe ₂ O ₃	10.96	9.78	13.12	3.12	3.41	8.87	6.66	4.77
MnO	0.16	0.17	0.18	0.12	0.12	0.16	0.18	0.14
MgO	3.96	4.73	3.17	0.98	1.49	3.77	3.26	2.11
CaO	5.30	6.05	5.82	3.46	3.67	4.59	6.21	4.25
Na ₂ O	4.51	5.31	4.53	4.24	4.11	2.49	2.51	2.96
K ₂ O	0.66	0.19	0.24	1.60	1.18	2.89	2.09	1.72
P ₂ O ₅	0.19	0.20	0.26	0.15	0.19	0.20	0.20	0.14
Sc	23.5	22.9	17.2	4.87		15.6	15.5	8.4
Ti	4582	3755	9399	1944		7197	4098	2565
V	186	177	148	27.8		72.6	135.2	45.0
Cr	19.3	56.9	42.1	24.5		17.4	73.9	51.6
Co	35.0	31.8	47.5	7.18		15.6	16.3	10.2
Ni	39.1	44.5	73.5	14.9		20.3	33.2	31.9
Rb	19.63	1.26	3.09	34.4		98.60	53.99	41.73
Sr	143	211	284	465		313	417	224
Y	17.60	15.00	23.25	5.30		18.90	12.38	8.13
Zr	132.40	100.29	203.50	98.85		64.30	99.85	118.33
Nb	5.66	5.05	13.35	3.70		11.30	4.01	5.33
Ba	266.30	39.65	128.90	421.31		639.00	594.33	423.67
La	25.46	6.59	32.15	17.61	12.5	16.80	20.75	12.87
Ce	52.12	17.84	68.00	33.90	25.3	37.60	45.18	22.37
Pr	6.19	2.69	8.93	4.17	2.76	4.79	5.75	3.14
Nd	23.58	12.09	35.40	14.47	9.56	19.20	23.69	11.13
Sm	4.38	2.93	6.91	2.29	1.63	4.28	4.55	2.24
Eu	1.18	0.82	1.83	0.62	0.32	1.13	1.22	0.68
Gd	3.85	2.76	5.97	1.64	1.01	3.95	3.46	1.90
Tb	0.59	0.42	0.83	0.20	0.13	0.59	0.47	0.25
Dy	3.07	2.49	4.57	0.92	0.59	3.25	2.37	1.49
Ho	0.63	0.52	0.90	0.17	0.12	0.67	0.47	0.29
Er	1.77	1.38	2.36	0.42	0.22	1.72	1.23	0.87
Tm	0.27	0.21	0.33	0.05	0.03	0.37	0.19	0.13
Yb	1.64	1.30	2.00	0.37	0.26	1.67	1.15	0.71
Lu	0.22	0.18	0.29	0.05	0.04	0.28	0.16	0.11
Hf	3.25	2.63	4.94	2.69		1.46	2.71	2.97
Ta	0.38	0.29	0.77	0.24		0.60	0.50	0.36
Th	5.77	4.30	3.39	2.53		2.66	3.18	3.03
U	0.93	0.85	0.57	0.57		0.48	0.41	0.44
La/Yb _N	10.51	3.47	10.85	32.13	32.45	6.79	12.30	13.67
La/Sm _N	3.66	1.42	2.94	4.89	4.83	2.47	2.87	3.77
Gd/Yb _N	1.90	1.71	2.41	3.67	3.14	1.91	2.44	2.37
Eu/Eu*	0.88	0.88	0.87	0.97	0.76	0.84	0.94	1.04

(continued on next page)

Table 6. (Continued)

Rock type	SAGm	SAGf	SDsubv	SRT	SRF	SRP	SDI	SGD
<i>n</i>	2	2	9	7	6	8	1	3
SiO ₂	66.90	73.26	67.27	74.62	77.01	76.55	60.01	69.18
TiO ₂	0.67	0.40	0.47	0.41	0.38	0.22	0.76	0.38
Al ₂ O ₃	15.39	14.38	16.98	15.40	15.77	14.34	19.49	16.17
Fe ₂ O ₃ *	5.15	2.70	3.65	2.09	0.80	1.68	5.91	3.97
MnO	0.13	0.13	0.14	0.12	0.12	0.12	0.15	0.14
MgO	2.95	1.08	1.71	0.72	0.62	0.99	1.93	1.11
CaO	3.95	3.83	4.39	1.94	1.86	1.92	6.07	3.50
Na ₂ O	2.70	3.40	3.58	2.06	1.82	1.40	3.66	3.27
K ₂ O	2.02	0.72	1.70	2.54	1.55	2.73	1.78	2.16
P ₂ O ₅	0.15	0.12	0.12	0.10	0.08	0.06	0.23	0.11
Sc	8.0	6.2	7.9	6.0	6.5	3.3	8.2	6.6
Ti	3432	2125	2052	1817	1800	1051	3990	1961
V	45.9	31.0	46.45	26.5	41.6	14.9	46.5	40.8
Cr	63.9	46.8	38.075	56.0	22.2	24.4	11.4	35.3
Co	13.5	6.8	10.995	5.5	3.3	3.5	12.2	8.5
Ni	57.6	33.2	28.55	19.3	10.2	15.4	10.1	22.1
Rb	53.21	18.07	42.6	86.10	36.20	67.44	42.80	53.64
Sr	240	264	437.25	151	262	199	487	318
Y	9.86	7.62	5.9	10.72	3.32	7.30	12.00	14.48
Zr	117.97	129.27	89.375	99.00	111.67	90.96	88.90	112.47
Nb	7.24	6.27	2.9025	6.01	3.46	10.00	6.59	6.41
Ba	691.36	283.44	379.5	544.50	293.17	456.16	509.00	513.01
La	13.71	11.50	15	36.00	14.76	31.29	18.70	20.31
Ce	28.00	20.19	26.75	51.00	28.30	63.59	37.40	38.42
Pr	3.33	2.57	3.4525	6.04	3.53	6.96	5.54	5.35
Nd	12.50	8.83	13.025	20.77	12.80	22.91	22.40	20.12
Sm	2.50	1.65	2.3	3.58	2.35	3.34	3.85	3.56
Eu	0.85	0.56	0.735	0.75	0.60	0.69	1.35	0.90
Gd	2.36	1.70	1.9375	2.81	1.87	2.50	3.22	2.96
Tb	0.36	0.22	0.2335	0.35	0.23	0.30	0.39	0.43
Dy	1.72	1.29	1.08825	1.64	0.90	1.23	2.03	2.32
Ho	0.34	0.25	0.22575	0.30	0.16	0.23	0.42	0.46
Er	0.89	0.34	0.5545	0.85	0.35	0.63	1.35	1.44
Tm	0.13	0.11	0.086575	0.13	0.05	0.09	0.21	0.22
Yb	0.72	0.67	0.4755	0.69	0.30	0.55	1.34	1.49
Lu	0.10	0.09	0.066525	0.11	0.04	0.08	0.21	0.24
Hf	3.08	2.90	2.3925	2.57	2.76	2.77	2.02	3.17
Ta	0.53	0.41	0.18475	0.38	0.23	0.71	0.43	0.72
Th	2.82	2.86	2.53	6.56	2.85	8.47	2.23	4.53
U	0.63	0.34	0.48425	0.87	0.62	1.97	0.18	1.14
La/Yb _N	12.96	11.58	21.299759	24.87	32.56	39.57	9.42	9.79
La/Sm _N	3.53	4.35	4.0811771	4.31	4.23	5.93	3.06	3.70
Gd/Yb _N	2.69	2.05	3.2786683	3.27	4.94	3.78	1.94	1.70
Eu/Eu*	1.06	1.03	1.0796298	0.79	0.92	0.73	1.17	0.87

(continued on next page)

Table 6. (Continued)

Note: n, number of analyses. Abbreviations: NA = Northern andesite suite, (+ E) 'enriched', (+ D) 'depleted' and (+ Nb) 'high-Nb' groups, respectively; NT and NTD = Northern tonalite and tonalitic dike; S = Southern andesite-dacite suite, (+ Nb) 'high-Nb', (+ A) andesite and (+ D) dacites, respectively; SAGm and SAGf = agglomerate textured volcanics, matrix and fragment, respectively; SD_{subv} = subvolcanic dacites; SRT, SRF and SRP = rhyolites: tuff, flow, and porphyry, respectively; SDI and SGD = Southern tonalite, diorite and granodiorite, respectively.

LREE ($\text{La}/\text{Sm}_N = 4.6\text{--}5.3$) contents and, conversely, by very low abundances of HREE ($\text{Gd}/\text{Yb}_N = 3.6\text{--}3.8$) and Y all similar to recent adakitic melts. It is widely accepted that adakite magmas result from melting of basaltic material at pressures high enough to stabilize garnet-amphibole \pm pyroxene \pm plagioclase in the melt residues (e.g., Drummond and Defant, 1990; Martin, 1999, and reference therein).

The Southern granodiorite suite includes largely dioritic (SDI) to granodioritic (SGD) plutonic rocks. In contrast to the Northern tonalite, they show apparently less fractionated REE patterns ($\text{La}/\text{Sm}_N = 3.2\text{--}4.1$, $\text{Gd}/\text{Yb}_N = 1.3\text{--}2.1$) and both Eu and Ti troughs (Fig. 24). Its somewhat older U-Pb zircon age in comparison with the other Khizovaara rocks (Fig. 2) implies that a crustal component could be involved to have formed this suite.

The Southern andesite-dacite-rhyolite suite occupies the southern limb of the Khizovaara structure. Based upon both the field appearance and available isotope-geochemical data it seems clear that the Iringora acid-felsic volcanics are close analogues of the Khizovaara Southern andesite-dacite-rhyolite suite. In terms of the major element chemistry their overall compositions make up mostly a calc-alkaline trend indicative of a mature volcanic arc. Amongst the latter high-Al andesite-dacitic compositions prevail. The common occurrence of agglomerate textured andesite-dacitic volcanics strongly suggests their emplacement in a subaerial environment.

The Southern andesite includes two distinct geochemical groups referred to here as the 'Southern andesite' group (SA) and the 'Southern high-Nb andesite' group (SANb). The first group together with the Southern dacites (SD) forms continuous trends on mostarker diagrams (Fig. 23). They are characterized by 0.6–0.9 wt% TiO_2 , 2.7–4.8 ppm Nb, low contents of Cr, Ni and Zr (Table 6), fractionated REE patterns ($\text{La}/\text{Sm}_N = 2.6\text{--}2$, $\text{Gd}/\text{Yb}_N = 2.0\text{--}2.7$) and pronounced Nb and Zr negative anomalies (Fig. 24). Dacites tend to have lower abundances of the major elements and Cr, Ni, V, Sc, Sr, REE while their LREE and HREE patterns are more and variably fractionated ($\text{La}/\text{Sm}_N = 3.0\text{--}4.7$, $\text{Gd}/\text{Yb}_N = 1.2\text{--}3.1$) in comparison to the andesites. The second group of andesites displays some enrichment in Nb (up to 11 ppm) and TiO_2 (up to 1.34 wt%), is rare in the population sample from the Southern suite. In contrast to the overall Southern andesite-dacite stem shows moderately fractionated REE patterns ($\text{La}/\text{Sm}_N = 2.5$, $\text{Gd}/\text{Yb}_N = 1.9$) and slight Nb and Zr negative anomalies. These high-Nb andesites being also markedly distinct from their Northern counterparts (cf. CA(Nb) and NA(Nb) in Table 6; Figs. 23, 24) are close in terms of major and trace abundances to the Nb-andesites of recent Western Pacific volcanic arcs (Prouteau et al., 2000).

Subvolcanic dacitic sills and dikes are an integral part of the Southern andesite-dacite-rhyolite suite. They plot along a compositional trend from high-Al dacite to rhyodacite (Fig. 23) close to fields of both the Southern volcanic counterparts and Northern tonalite. In contrast to the former, the subvolcanic dacites show stronger fractionated REE patterns with lower HREE contents ($\text{La}/\text{Sm}_N = 3.8\text{--}4.3$, $\text{Gd}/\text{Yb}_N = 3.1\text{--}3.5$) and higher Sr/Y and Sr/Nb (Fig. 24) ratios all indicative of adakitic magmas (e.g., Martin, 1999).

Rhyolites occur as small sill-like bodies and tuffaceous horizons. The subvolcanic rhyolites are dominantly porphyritic in texture, with plagioclase and quartz phenocrysts up to few mm long. Compositionally these display a compact field of high siliceous K-Na rhyolites (Fig. 22). Their REE patterns are strongly fractionated ($\text{La}/\text{Sm}_N = 5.5\text{--}6.5$, $\text{Gd}/\text{Yb}_N = 3.3\text{--}4.5$) and characterized by pronounced negative Eu spikes. Most of the HFSE, as well as Sr, show a marked depletion, whereas U, Th and Nb demonstrate a clear enrichment relative to abundances of the neighbouring trace elements (Fig. 24). Trends to lower Al_2O_3 , CaO, Na_2O and Sr with increasing silica from 74 to 79 wt% must primarily reflect removal of quartz and plagioclase, which is consistent with the presence of these minerals as phenocrysts. In contrast to the subvolcanic counterparts, the felsic tuffaceous horizons show an abnormal enrichment of Al_2O_3 (up to 18 wt%). For individual samples, high abundances of Ni and Cr coupled together with irregular variations of Al_2O_3 , Ti, Zr, Nb and Th appear to reflect a non-magmatic component, either hydrothermal or sedimentary, was involved in their petrogenesis.

Based on the geochemical ground and petrological constraints it should be emphasized that the felsic rocks could not have evolved from any partially melted mafic precursors by fractional crystallization alone. This requires either a different magma source or an addition of enriched siliceous component during the evolution from intermediate to felsic composition. A possible source for such melts could be genetically related with the both suites of adakitic affinity, the Southern andesite-dacite volcanics and the Northern tonalite. Indeed, as has been experimentally shown recently (Prouteau et al., 1999), rhyolitic compositions close to the above might be produced by $\sim 30\%$ crystal fractionation of a rising hydrous adakitic magma. This checks well with evidence for major- and trace-element chemistry of the Southern agglomerate textured volcanics. Compositionally, the matrix of the agglomerate lavas (SAGm) is similar to the average Southern subvolcanic dacite (SDsubv) of adakitic affinity while their fragments (SAGf) tend to be akin to the rhyolitic flow (SRF) (Table 6).

In summary, although the Northern and Southern volcanic suites display different geochemical features, all the above compositional varieties could result from partial melting of either the mantle wedge or an oceanic slab, as well as through a combination of these processes. Indeed, it is commonly believed that high-Al andesite-dacite volcanics result from partial melting of hydrated mantle wedge whereas adakitic melts developed through the partial melting of oceanic slab. Origin of Nb-enriched andesites is interpreted in a variety of ways each being explained by interaction between a subarc mantle peridotite and adakitic liquids (Sajona et al., 2000). A similar group of andesitic volcanics has been described in the 2.7 Ga Wawa greenstone belt, Superior Province, Canada by Polat and Kerrich (2001, 2004). It is important that recent adakitic and

Nb-enriched andesite occurrences are clearly associated with the subduction of young, hot oceanic lithosphere (e.g., Drummond and Defant, 1990; Drummond et al., 1996; Sajona et al., 2000; Prouteau et al., 2000) that is known to be important in the genesis of recent boninite occurrences as well (Pearce et al., 1992).

4. CONCLUSIONS AND GEODYNAMIC IMPLICATIONS

Several lines of evidence suggest that the North Karelian greenstone belt contains remnants of a 2.8 Ga SSZ ophiolite association. The Iringora sequence display partially preserved ophiolite-like pseudostratigraphy including lava, sheeted dike and layered gabbro units, whereas the original ophiolitic stratigraphy of the Khizovaara Structure is obscured by both a carapace of the acid-felsic arc-related volcanics, and later tectonic imbricate events. Remnants of sheeted dikes and their transitions into both the lava and the gabbro units are preserved within the Iringora sequence. Sheeted dikes are one of the straight forward indicators for the interpretation of such extensional magmatic system as an ophiolite. Although sheeted dikes may be developed during rifting of volcanic edifices built even on sialic crustal basement, those of the Iringora sequence, combined with their explicit geochemical features, strongly suggest its SSZ ophiolite nature. This ophiolitic complex has experienced intense structural and high-pressure metamorphic transformations during, at least, two distinct tectonic stages, including Neoproterozoic (2.8–2.7 Ga ago) and Paleoproterozoic (1.9–1.75 Ga ago). The original layered structure was largely disrupted to an extent that we cannot construct a composite section through the Iringora sequence in order to assess a possible crustal thickness of the ophiolite.

Nonetheless, significant information comes from the geochemical and isotope data for the NKGB boninite series and related rocks. Their major and trace element abundances were not largely affected by the post-magmatic alteration processes retaining, therefore, records of the petrogenetic processes appropriate to tectonic implications. We have noted that the 2.8 Ga NKGB boninite series are remarkably similar compositionally to the upper pillow lavas from the Troodos ophiolite, a much younger example of high-Ca boninite series (Crawford et al., 1989). The amazing similarities in major and trace element chemistry along the boninite series of manifestly different ages reflect their similar petrogenic history. This implies, in turn, that a tectonic setting of the North Karelian boninite series volcanism was not substantially different from that of recent analogues.

Thrusting of the Iringora ophiolitic sequence onto the arc assemblage resulted from an arc-trench interaction (Figs. 7, 12). This could have occurred in a setting of forearc extension that seems typical for most of Phanerozoic SSZ ophiolite assemblages (e.g., Becaluva and Serri, 1988; Pearce et al., 1992; Stern and Bloomer, 1992). Recently Shervais (2001) summarized a wealth of geologic evidence on the most-known SSZ ophiolites and concluded "that suprasubduction zone ophiolites display a consistent sequence of events during their formation and evolution that demonstrates that they must form in response to processes that are common to all such ophiolites and are characteristic of their mode of

Table 7. Comparison of the geological characteristics of Phanerozoic SSZ ophiolites and the Neoproterozoic SSZ ophiolite-like sequences of the North Karelian greenstone belt. The stages of the life cycle of SSZ ophiolites and their geological characteristics after Shervais (2001)

	Stage 1: Birth	NKGB	Stage 2: Youth	NKGB	Stage 3: Maturity	NKGB	Stage 4: Death	NKGB	Stage 5: Resurrection	NKGB
Events	initial spreading, hinge rollback	inferred	refractory melts, second stage melting	present	calc-alkaline, "normal" arc	present	ridge subduction or directly to obduction	ridge subduction (?)	obduction onto passive margin (Tethyan) or accretionary uplift (Cordilleran)	accretionary uplift (Cordilleran)
Volcanic rocks	primitive arc tholeiites (basalt to basaltic-andesite)	present	high-Mg andesites, boninites, tholeiitic ankaramites	present	andesite, dacite, basaltic andesite	present	MORB-like or OIB	present	none	none
Plutonic rocks	layered gabbro, troctolite, dunite	not observed	wehrlite-Cpxite sill complex	present (Kozhevnikov, pers. com.)	quartz diorite, hornblende diorite, agmatites	present	none	present	rare granitoids; anatexis of lower plate	present
Meta-morphic rocks	hydrothermal alteration of volcanics	inferred	hydrothermal alteration of volcanics	inferred	hydrothermal alteration of volcanics	present	high-grade metamorphic sole	inferred	obduction may be cold or hot, new subduction zone may form (accretionary uplift)	hot obduction (?)

Abbreviations: NKGB, North Karelian Greenstone belt; MORB, mid-ocean ridge basalts; OIB, ocean island basalts.

formation". Comparison the main geologic characteristics of the Neoproterozoic North Karelian ophiolite-like sequences with those from the stages of the Shervais 'Life cycle of SSZ ophiolite' shows (Table 7) that the most, if not all, of distinctive features of SSZ are either present in the 2.8 Ga NKGB or may be inferred. This implies that a mode of formation and evolution of the Neoproterozoic SSZ ophiolite-like rocks was very similar to the Phanerozoic SSZ ophiolites. A corollary from this comparison is that a modern subduction style accompanied by a spreading of previously formed oceanic lithosphere operated in the Neoproterozoic.

ACKNOWLEDGEMENTS

This work was supported by the RFBR (grants 990565607, 990564055, 000564295 and 00056401). The underlying field work for this study were mostly funded by the Geological Institute of the Russian Academy of Sciences. The main analytical procedures to date zircons by conventional method were done by T.V. Gracheva, T.I. Kirnozova and V.A. Makarov at the Vernadsky Institute of Geochemistry and Analytical Chemistry of RAS, Moscow. Elena Bibikova is grateful to Dr. S. Claesson from the Swedish Royal Museum of Natural History, Stockholm, for providing access to the ion microprobe NORDSIM technique. The authors would especially like to thank Dr. I. Puchtel for the isotope studies of samples.

REFERENCES

- Abbott, D.H., Drury, R., Smith, W.H.F., 1994. Flat to steep transition in subduction style. *Geology* 22, 937–940.
- Amelin, Yu.V., Heaman, L.M., Semenov, V.S., 1995. U-Pb geochronology of layered mafic intrusions in the eastern Baltic Shield: implication for the timing and duration of Paleoproterozoic continental rifting. *Precambrian Research* 75, 31–46.
- Arndt, N.T., Albarède, F., Nisbet, E.G., 1997. Mafic and Ultramafic magmatism. In: de Wit, M., Ashwal, L.D. (Eds.), *Greenstone Belts*. In: *Oxford Monographs on Geology and Geophysics*, vol. 35, pp. 233–254.
- Arnold, J., Powell, R., Sandiford, M., 2000. Amphibolites with staurolite and other aluminous minerals: calculated mineral equilibria in NCFMASH. *Journal of Metamorphic Geology* 18, 23–40.
- Babarina, I.I., 1998. Structural evolution of the Lake Kukas segment, North Karelia collision zone. *Geotektonika* 3, 80–96.
- Beccaluva, L., Serri, G., 1988. Boninitic and low-Ti subduction-related lavas from intraoceanic arc-back-arc systems and low-Ti ophiolites: a reappraisal of their petrogenesis and original tectonic setting. *Tectonophysics* 146, 291–315.
- Bibikova, E.V., Skiöld, T., Bogdanova, S.V., Gorbachev, R., Slabunov, A., 2001. Titanite-rutile thermochronometry across the boundary between the Archaean Craton in Karelia and the Belomorian Mobile Belt, eastern Baltic Shield. *Precambrian Research* 105, 315–330.

- Bibikova, E.V., Skiöld, T., Bogdanova, S.V., 1996. Age and geodynamic aspects of the oldest rocks in the Precambrian Belomorian belt, Baltic Shield. *Geological Society of London Special Publication* 112, 58–96.
- Bickle, M.J., Nisbet, E.G., Martin, A., 1994. Archean greenstone belts are not oceanic crust. *Journal of Geology* 102, 121–138.
- Bogdanova, S.V., 1996. High-grade metamorphism of 2.45–2.4 Ga age in mafic intrusions of the Belomorian Belt in the northeastern Baltic Shield. *Geological Society of London Special Publication* 112, 69–90.
- Bridgwater, D., Scott, D.J., Balagansky, V.V., Timmerman, M.J., Marker, M., Bushmin, S.A., Alexeyev, N.L., Daly, J.S., 2001. Age and provenance of early Precambrian metasedimentary rocks in the Lapland-Kola Belt, Russia: evidence from Pb and Nd isotopic data. *Terra Nova* 13, 32–37.
- Cameron, W.E., 1985. Petrology and origin of primitive lavas from the Troodos ophiolite, Cyprus. *Contributions to Mineralogy and Petrology* 89, 239–255.
- Cameron, W.E., Nisbet, E.G., Dietrich, V.J., 1979. Boninites, komatiites and ophiolitic basalts. *Nature* 280, 550–553.
- Condie, K.C., Viljoen, M.J., Kable, E.D.J., 1977. Effects of alteration on element distributions in Archean tholeiites from the Barberton greenstone belt, South Africa. *Contributions to Mineralogy and Petrology* 64, 75–89.
- Crawford, A.J., Fallon, T.J., Green, D.H., 1989. Classification, petrogenesis and tectonic setting of boninites. In: Crawford, A.J. (Ed.), *Boninites*. Unwin Hyman, London, pp. 2–44.
- Drummond, M.S., Defant, M.J., 1990. A model for trondhjemite-tonalite-dacite genesis and crustal growth via slab melting: Archean to modern comparisons. *Journal of Geophysical Research* 95, 21503–21521.
- Drummond, M.S., Defant, M.J., Kepezhinskas, P.K., 1996. Petrogenesis of slab-derived trondhjemite-tonalite-dacite/adakite magmas. *Geological Society of America Special Paper* 315, 205–215.
- Duncan, R.A., Green, D.H., 1980a. The genesis of refractory melts in the formation of oceanic crust. *Contributions to Mineralogy and Petrology* 96, 326–342.
- Duncan, R.A., Green, D.H., 1980b. Role of multistage melting in the formation of oceanic crust. *Geology* 8, 22–26.
- Elton, D., 1989. Pressure of origin of primary mid-ocean-ridge basalts. In: Saunders, A.D., Norry, M.J. (Eds.), *Magmatism in the Ocean Basins*. Geological Society of London Special Publication 42, 125–136.
- Fallon, T.J., Crawford, A.J., 1991. The petrogenesis of high-calcium boninite lavas dredged from the northern Tonga ridge. *Earth and Planetary Science Letters* 102, 375–394.
- Fan, J., Kerrich, R., 1997. Geochemical characteristics of Al-depleted and undepleted komatiites and HREE-enriched tholeiites, western Abitibi greenstone belt: variable HFSE/REE systematics in a heterogeneous mantle plume. *Geochimica et Cosmochimica Acta* 61, 4723–4744.
- Fed'kin, V.V., 1975. *Staurolites*. Nauka, Moscow, p. 465 (in Russian).
- Fed'kin, V.V., Aranovich, L.Y., 1990. The Empirical Refinement of the Staurolite-Garnet Geothermometer; Experiment-89. Nauka, Moscow, pp. 41–43.
- Flower, M.F.L., Levine, H.M., 1987. Petrogenesis of a tholeiite-boninite sequence from Ayios Mamas, Troodos ophiolite: evidence for splitting of a volcanic arc. *Contributions to Mineralogy and Petrology* 97, 509–524.
- Gaál, G., Gorbatshev, R., 1987. An outline of the Precambrian evolution of the Baltic Shield. *Precambrian Research* 35, 15–52.

- Green, T.H., Blundy, J.D., Adam, J., Yaxley, G.M., 2000. SIMS determination of trace element partition coefficients between garnet, clinopyroxene and hydrous basaltic liquids at 2–7.5 Gpa and 1080–1200 °C. *Lithos* 53, 165–187.
- Hickey, R.L., Frey, F.A., 1982. Geochemical characteristics of boninite series volcanics: Implications for their source. *Geochimica et Cosmochimica Acta* 46, 2099–2115.
- Hirose, K., Kushiro, I., 1993. Partial melting of dry peridotites at high pressures: determination of compositions of melts segregated from peridotite using aggregates of diamond. *Earth and Planetary Science Letters* 102, 477–489.
- Hofmann, A.W., 1988. Chemical differentiation of the Earth: The relationship between mantle continental crust and oceanic crust. *Earth and Planetary Science Letters* 90, 297–314.
- Holland, T., Blundy, J., 1994. Non-ideal interactions in calcic amphiboles and their bearing on amphibole-plagioclase thermometry. *Contributions to Mineralogy and Petrology* 116, 433–447.
- Jochum, K.P., Arndt, N.T., Hofmann, A.W., 1990. Nb-Th-La in komatiites and basalts: constraints on komatiite petrogenesis and mantle evolution. *Earth and Planetary Science Letters* 107, 272–289.
- Kerrick, R., Wyman, D., Fan, J., Bleeker, W., 1998. Boninite series: low Ti-tholeiite associations from the 2.7 Ga Abitibi greenstone belt. *Earth and Planetary Science Letters* 164, 303–316.
- Koch-Müller, M., 1997. Experimentally determined Fe-Mg exchange between synthetic staurolite and garnet in the system MgO-FeO-Al₂O₃-SiO₂-H₂O. *Lithos* 41, 185–212.
- Kozhevnikov, V.N., 2000. Archean Greenstone Belts of the Karelian Craton as Accretionary Orogens. Karelian Science Center, Petrozavodsk, p. 223 (in Russian).
- Kozhevnikov, V.N., 1992. Geology and Geochemistry of the Archean North Karelian Greenstone Structures. Karelian Science Center, Petrozavodsk, p. 199 (in Russian).
- Koziol, A.M., Newton, R.C., 1989. Grossular activity-composition relationship in ternary garnets determined by reversed displaced-equilibrium experiments. *Contributions to Mineralogy and Petrology* 103, 423–433.
- Kretz, R., 1983. Symbols for rock-forming minerals. *American Mineralogist* 68, 277–279.
- Kushiro, I., 1990. Partial melting of mantle wedge and evolution of island arc crust. *Journal of Geophysical Research* 95, 15929–15939.
- Kusky, T.M., Li, J.H., Tucker, R.D., 2001. The Archean Dongwanzi ophiolite complex, North China Craton: 2.505-Billion-Year-Old oceanic crust and mantle. *Science* 292, 1142–1145.
- Kusky, T.M., Vearncombe, J.R., 1997. Structural Aspects. In: de Wit, M., Ashwal, L.D. (Eds.), *Greenstone Belts*. In: *Oxford Monographs on Geology and Geophysics*, vol. 35, pp. 91–124.
- Le Bas, M.J., 2000. IUGS reclassification of the high-Mg and picritic volcanic rocks. *Journal of Petrology* 41, 1467–1470.
- Lobach-Zhuchenko, S.B., Chekulaev, V.P., Sergeev, S.A., Levchenkov, O.A., Krylov, I.N., 1993. Archean rocks from southeastern Karelia (Karelian granite-greenstone terrain). *Precambrian Research* 62, 375–397.
- Ludden, J., Gelinas, L., Trudel, P., 1982. Archean metavolcanics from the Rouyn-Noranda district, Abitibi greenstone belt, Quebec: 2. Mobility of trace elements and petrogenetic constraints. *Canadian Journal of Earth Sciences* 19, 2276–2287.
- Martin, H., 1999. Adakitic magmas: modern analogues of Archean granitoids. *Lithos* 46, 411–429.
- Martin, H., 1986. Effect of steeper Archean geothermal gradient on geochemistry of subduction zone magmas. *Geology* 14, 753–756.
- McKenzie, D., Bickle, M.J., 1988. The volume and composition of melt generated by extension of the lithosphere. *Journal of Petrology* 29, 625–629.
- McCulloch, M., 1993. The role of subducted slabs in an evolving earth. *Earth and Planetary Science Letters* 115, 89–100.

- McCulloch, M.T., Gamble, J.A., 1991. Geochemical and geodynamical constraints on subduction zone magmatism. *Earth and Planetary Science Letters* 102, 358–374.
- Meffre, S., Aitchison, J.C., Crawford, A.J., 1996. Geochemical evolution and tectonic significance of boninites and tholeiites from the Koh ophiolite, New Caledonia. *Tectonics* 15, 67–83.
- Meijer, A., 1980. Primitive arc volcanism and a boninite series: examples from Western Pacific island arc. In: Hayes, D.E. (Ed.), *The Tectonic and Geologic Evolution of Southeast Asian Sea and Islands*. In: *Geophysical Monographs*, vol. 23, pp. 269–282.
- Miller, Yu.V., Mil'kevich, R.I., 1995. Thrust-fold structure of the Belomorian zone and its correlation with the Karelian granite-greenstone region. *Geotektonika* 6, 80–93.
- Moores, E.M., Twiss, R.J., 1995. *Tectonics*. W.H. Freeman and Co., New York, p. 414.
- Moscovchenko, N.I., Turchenko, S.I., 1975. Metamorphism of Kyanite-Sillimanite Type and Sulphidic Ores (Northern Karelia). *Nauka, Leningrad*, p. 137 (in Russian).
- Natland, J.H., 1981. Crystal morphologies and pyroxene compositions in boninites and tholeiitic basalts from Deep Sea Drilling Project Holes 458 and 459B in the Mariana fore-arc region. *Initial Reports of the Deep Sea Drilling Project* 60, pp. 681–707.
- Newton, R.C., Haselton, H.T., 1981. Thermodynamics of the garnet-plagioclase- Al_2SiO_5 -quartz geobarometer. In: Newton, R.C., Navrotsky, A., Wood, B.J. (Eds.), *Thermodynamics of Minerals and Melts*. Springer, New York, pp. 131–147.
- Ohnenstetter, D., Brown, W.L., 1996. Boninites: a review. In: Demaiffe, D. (Ed.), *Petrology and Geochemistry of Magmatic Suites of Rocks in the Continental and Oceanic Crust. A Volume Dedicated to Professor Jean Michot, Université Libre de Bruxell*. Royal Museum for Central Africa, Tervuren, pp. 307–320.
- Pearce, J.A., Lippard, S.J., Roberts, S., 1984. Characteristics and tectonic significance of supra-subduction zone ophiolites. In: Kokelaar, B.P., Howells, M.F. (Eds.), *Geological Society of London Special Publication* 16, 77–94.
- Pearce, J.A., Kempton, P.D., Nowell, G.M., Noble, S.R., 1999. Hf-Nd element and isotope perspective on the nature and provenance of mantle and subduction components in Western Pacific arc-basin systems. *Journal of Petrology* 40, 1579–1611.
- Pearce, J.A., van der Laan, S.R., Arculus, R.J., Murton, B.J., Ishii, T., Peate, D.W., Parkinson, I.J., 1992. Boninite and harzburgite from leg 125 (Bonin-Mariana forearc): a case study of magma genesis during the initial stages of subduction. *Proceedings of the Ocean Drilling Program, Scientific Results* 125, 623–659.
- Perchuk, L.L., 1989. Intercorrelation of Fe-Mg geothermometers using the Nernst law. *Geokhimiya* 5, 611–622.
- Poidevin, J.-L., 1994. Boninite-like rocks from the Palaeoproterozoic greenstone belt of Bogoin, Central African Republic: Geochemistry and petrogenesis. *Precambrian Research* 68, 97–113.
- Polat, A., Kerrich, R., 2001. Magnesian andesites, Nb-enriched basalt-andesites, and adakites from late-Archean 2.7 Ga Wawa greenstone belts, Superior Province, Canada: implication for late Archean subduction zone petrogenetic processes. *Contributions to Mineralogy and Petrology* 141, 36–52.
- Polat, A., Kerrich, R., 2004. Precambrian arc associations: Boninites, adakites, magnesian andesites, and Nb-enriched basalts. In: Kusky, T.M. (Ed.), *Precambrian Ophiolites and Related Rocks*. In: *Developments in Precambrian Geology*, vol. 13. Elsevier, Amsterdam, pp. 567–597.
- Prouteau, G., Maury, R.C., Sajona, F.G., Cotton, J., Joron, J.-L., 2000. Behavior of niobium, tantalum and other high field strength elements in adakites and related lavas from the Philippines. *The Island Arc* 9, 487–498.

- Prouteau, G., Scaillet, B., Pichavant, M., Maury, R.C., 1999. Fluid-present melting of ocean crust in subduction zones. *Geology* 27, 1111–1114.
- Puchtel, I.S., Haase, K.M., Hofmann, A.W., Chauvel, C., Kulikov, V.S., Garbe-Schönberg, C.-D., Nemchin, A.A., 1997. Petrology and geochemistry of crustally contaminated komatiitic basalts from the Vetryny Belt, southeastern Baltic Shield: Evidence for an early Proterozoic mantle plume beneath rifted Archean continental lithosphere. *Geochimica et Cosmochimica Acta* 61, 1205–1222.
- Puchtel, I.S., Hofmann, A.W., Amelin, Yu.V., Garbe-Schönberg, C.-D., Samsonov, A.V., Shchipansky, A.A., 1999. Combined mantle plume-island arc model for the formation of the 2.9 Ga Sumozero-Kenozero greenstone belt, SE Baltic Shield: Isotope and trace element constraints. *Geochimica et Cosmochimica Acta* 63, 3579–3595.
- Puchtel, I.S., Hofmann, A.W., Mezger, K., Shchipansky, A.A., Samsonov, A.V., 1998. Oceanic plateau for continental crustal growth in the Archean: a case study from the Kostomuksha greenstone belt, Nw Baltic Shield. *Earth and Planetary Science Letters* 155, 57–74.
- Riganti, A., Wilson, A.H., 1995. Geochemistry of the mafic/ultramafic volcanic associations of the Nondweni greenstone belt, South Africa, and constraints on their petrogenesis. *Lithos* 34, 235–252.
- Sajona, F.G., Maury, R.C., Prouteau, G., Cotton, J., Schiano, P., Bellon, H., Fontaine, L., 2000. Slab melt as metasomatic agent in island arc magma mantle sources, Negros and Batan (Philippines). *The Island Arc* 9, 472–486.
- Shchipansky, A.A., Babarina, I.I., Krylov, K.A., Samsonov, A.V., Bogina, M.M., Bibikova, E.V., Slabunov, A.I., 2001. The oldest ophiolites: the late Archean suprasubduction zone complex of the Iringora structure, North Karelian greenstone belt. *Doklady Earth Science* 377a, 283–287.
- Shchipansky, A.A., Samsonov, A.V., Bogina, M.M., Slabunov, A.I., Bibikova, E.V., 1999. High-Mg, low-Ti quartz amphibolites of the Khizovaara greenstone belt, Northern Karelia: Archean metamorphosed boninites? *Doklady Earth Science* 365a, 817–820.
- Shervais, J.W., 2001. Birth, death, and resurrection: The life cycle of suprasubduction zone ophiolites. *Geochemistry, Geophysics, Geosystems* 2, 2000GS000080.
- Shervais, J.W., 1982. Ti-V plots and petrogenesis of modern and ophiolitic lavas. *Earth and Planetary Science Letters* 59, 101–118.
- Smellie, J.L., Stone, P., Evans, J., 1995. Petrogenesis of boninites in the Ordovician Ballantrae Complex ophiolite, southwestern Scotland. *Journal of Volcanology and Geothermal Research* 69, 323–342.
- Sobolev, A.V., Danyushevsky, L.V., 1994. Petrology and geochemistry of boninites from the north termination of the Tonga trench: constraints on the generation conditions of primary high-Ca boninite magmas. *Journal of Petrology* 35, 1183–1211.
- Sobolev, A.V., Portnyagin, M.V., Dmitriev, L.V., Tsamerian, O.P., Danyushevsky, L.V., Kononkova, N.N., Shimizu, N., Robinson, P.T., 1993. Petrology of ultramafic lavas and associated rocks of the Troodos Massif, Cyprus. *Petrology* 1, 331–361.
- Sorjonen-Ward, P., Nironen, M., Luukkonen, E., 1997. Greenstone associations in Finland. In: de Wit, M., Ashwal, L.D. (Eds.), *Greenstone Belts*. In: *Oxford Monographs on Geology and Geophysics*, vol. 35, pp. 676–698.
- Staudigel, H., Tauxe, L., Gee, J.S., Bogaard, P., Haspels, J., Kale, G., Meijer, P., Swaak, B., Tuin, M., Van Soest, M.C., Verdurmen, E.A.Th., Zevenhuizen, A., 1999. Geochemistry and intrusive directions in sheeted dikes in the Troodos ophiolite: Implications for Mid-ocean ridge spreading centers. *Geochemistry, Geophysics, Geosystems* 1, 1999GS000001.

- Stein, E., Dietl, C., 2001. Hornblende thermobarometry of granitoids from the Central Odenwald (Germany) and their implications for the geotectonic development of the Odenwald. *Mineralogy and Petrology* 72, 185–207.
- Stern, R.J., Bloomer, S.H., 1992. Subduction zone infancy: Examples from the Eocen Izu-Bonin-Mariana and Jurassic California arcs. *Geological Society of America Bulletin* 104, 1621–1636.
- Sylvester, P.J., Harper, G.D., Byerly, G.R., Thurston, P.S., 1997. Volcanic aspects. In: de Wit, M., Ashwal, L.D. (Eds.), *Greenstone Belts*. In: *Oxford Monographs on Geology and Geophysics*, vol. 35, pp. 55–90.
- Sun, S.-s., Nesbitt, R.W., 1978. Geochemical regularities and genetic significance of ophiolitic basalts. *Geology* 6, 689–693.
- Sun, S.-s., Nesbitt, R.W., McCulloch, M.T., 1989. Geochemistry and petrogenesis of Archaean and early Proterozoic siliceous high-magnesium basalts. In: Crawford, A.J. (Ed.), *Boninites*. Unwin Hyman, London, pp. 148–173.
- Thurston, P.S., Kozhevnikov, V.N., 2000. An Archean quartz arenite-andesite association in the eastern Baltic Shield, Russia: implications for assemblage types and shield history. *Precambrian Research* 101, 313–340.
- Walker, D., Shibata, T., De Long, S.E., 1979. Abyssal tholeiites from the Oceanographic fracture zone II, phase equilibria and mixing. *Contributions to Mineralogy and Petrology* 70, 111–125.
- Whitehouse, M., Claesson, S., Sunde, T., Vestin, J., 1997. Ion microprobe U-Pb zircon geochronology and correlation of Archaean gneisses from the Lewisian Complex of Gruinard Bay, north-western Scotland. *Geochimica et Cosmochimica Acta* 61, 4429–4438.
- Wyman, D.A., 1999. Paleoproterozoic boninites in an ophiolite-like setting, Trans-Hudson orogen, Canada. *Geology* 27, 455–458.